# Numerical Methods for the QCD Overlap Operator IV: Hybrid Monte Carlo

N. Cundy, <sup>a</sup> S. Krieg, <sup>a</sup> G. Arnold, <sup>c</sup> A. Frommer, <sup>b</sup> Th. Lippert<sup>c, a</sup> and K. Schilling <sup>a</sup>

<sup>a</sup>Department of Physics, University of Wuppertal, Germany.

<sup>b</sup>Department of Mathematics, University of Wuppertal, Germany.

<sup>c</sup>John von Neumann Institute for Computing, Jülich Research Centre, 52425

Jülich, Germany.

#### Abstract

The extreme computational costs of calculating the sign of the Wilson matrix within the overlap operator have so far prevented four dimensional dynamical overlap simulations on realistic lattice sizes, because the computational power required to invert the overlap operator, the time consuming part of the Hybrid Monte Carlo algorithm, is too high. In this series of papers we introduced the optimal approximation of the sign function and have been developing preconditioning and relaxation techniques which reduce the time needed for the inversion of the overlap operator by over a factor of four, bringing the simulation of dynamical overlap fermions on medium-size lattices within the range of Teraflop-computers.

In this paper we adapt the HMC algorithm to overlap fermions. We approximate the matrix sign function using the Zolotarev rational approximation, treating the smallest eigenvalues of the Wilson operator exactly within the fermionic force. We then derive the fermionic force for the overlap operator, elaborating on the problem of Dirac delta-function terms from zero crossings of eigenvalues of the Wilson operator. The crossing scheme proposed shows energy violations which are better than  $O(\Delta \tau^2)$  and thus are comparable with the violations of the standard leapfrog algorithm over the course of a trajectory. We explicitly prove that our algorithm satisfies reversibility and area conservation. Finally, we test our algorithm on small  $4^4$ ,  $6^4$ , and  $8^4$  lattices at large masses.

Key words: Lattice Quantum Chromodynamics, Overlap Fermions, Hybrid Monte Carlo

PACS: 02.50, 11.15.H, 12.38.G, 11.30.R

#### 1 Introduction

For two decades numerical simulations of very light quarks within lattice quantum chromodynamics have remained intractable as the chiral symmetry of the underlying QCD Lagrangian, which holds in the case of zero mass quarks, could not be embedded into flavour conserving fermion lattice discretisation schemes. The standard workaround took recourse to simulations with fairly heavy quarks instead and extrapolated the results over a wide range of quark masses to the very light quark mass regime. Unfortunately, simulating far beyond the realm of chiral perturbation theory such extrapolations carry large systematic errors. These errors have to be avoided in order to achieve a sufficient precision of phenomenological observables.

During the 90's the first lattice chiral Dirac operators were written down. While studying domain wall fermions [2], an early attempt to simulate chiral fermions on the lattice, Neuberger and Narayanan realised that the Nielson-Ninomiya theorem [3] could be circumvented by placing an infinite number of fermions on the lattice. This insight led them to the overlap lattice Dirac operator [4,5]. Afterwards, Hasenfratz, while working with classically perfect fermions, realised that the small mass bottleneck could be overcome by using a discretisation scheme that obeys a lattice variant of chiral symmetry [6], as expressed by the Ginsparg-Wilson relation for the quark propagator [7], which in turn implies a novel version of chiral symmetry on the lattice [8]. The overlap operator obeys the Ginsparg-Wilson relation. Theoretically, such a scheme induces a dramatic reduction in fluctuations in the vicinity of zero quark mass, but the implementation of the overlap operator requires the solution of linear systems involving the inverse matrix square root or the matrix sign function (of the hermitian Wilson-Dirac operator Q).

The problem of approximating the action of  $\operatorname{sign}(Q)$  on a vector has been discussed in a number of papers, using polynomial approximations [9,10,11,12,13], Lanczos based methods [14,15,16,17] and multi-shift CG combined with a partial fraction expansion [18,19,20,21]. The Zolotarev partial fraction approximation (ZPFE), first applied to lattice QCD in [22] - the first paper in the present series - is the optimal approximation to the matrix sign function. ZPFE has led to an improvement of over a factor of 3 compared to the Chebyshev polynomial approach [11]. This technique to compute the sign function has meanwhile been established as the method of choice, [23,24,25]. Moreover, it is the natural starting point for both the treatment of dynamical overlap fermions [26] and optimised domain wall fermions [27,28,29]  $^1$ .

 $<sup>^1</sup>$  An alternative is to use a 5-dimensional representation of the overlap operator - see [30,31,32]. An HMC algorithm using a polynomial approximation to the sign

Until recently, simulations with overlap fermions were restricted to the quenched model where fermion loops are neglected [34,35,36,37], or hybrid calculations using staggered or Wilson sea quarks, because of the sheer costs of the evaluation of sign functions of matrices with extremely high dimensions. The challenge today is to go beyond the quenched model and include dynamical fermions. At this point we have the unique challenge to devise optimised simulation algorithms for overlap fermions, investigating novel numerical and stochastical techniques.

In this paper, we look at the details of applying the Hybrid Monte Carlo algorithm [38] - a standard method for simulating dynamical fermions on the lattice - to overlap fermions<sup>2</sup>. Earlier work done concerning dynamical overlap fermions in the Schwinger model can be found in [40,41,42,43]. More recently, there have been some exploratory works in full QCD [26,44,45]. For the most part we just need to adapt the algorithm for (for example) Wilson fermions. However the discontinuity in the matrix sign function used in the overlap construction causes additional complications: as soon as one of the eigenvalues of Q crosses zero, the change in the sign of the eigenvalue leads to a discontinuity in the fermionic part of the action, which induces a Dirac delta function in the HMC fermionic force, as first discussed in [26,44]. This effect is predominently seen in strong coupling: eigenvalue crossings are rare in the weak coupling limit [46].

The major part of this paper will deal with the proper integration of this singular force term under integration. The most important improvements in our study are: (1) We calculate the energy violation at the crossing exactly; (2) We discuss the implementation of the eigenvalue projection technique in the HMC algorithm; (3) We discuss what happens when two eigenvalues cross in the same molecular dynamics step; and (4) we use a momentum update when there is an eigenvalue crossing with improved energy consevation properties, with the leading errors now  $O(\Delta \tau^2)$ .

The main practical difficulty in running dynamical overlap simulations is the cost in computer time. Overlap fermions are at least O(100) times more expensive to compute than Wilson fermions. In other papers in this series [47,48,49], we discussed how the inversion of the overlap operator, the time consuming part of the HMC algorithm, can be accelerated. Here we will use these methods, and estimate the time required with our current algorithms for a full HMC simulation on moderate lattices at realistic masses. Our early results are outlined in [50].

function was tested in [33], and found to be inferior to the ZPFE.

<sup>&</sup>lt;sup>2</sup> It has also been suggested that one could use improved staggered fermions for the molecular dynamics and overlap fermions for the HMC accept/reject step [39]. It is unclear whether or not this will lead to an unacceptably low acceptance rate.

Section 2.1 gives a brief introduction to the Hybrid Monte-Carlo method for generating dynamical configurations. Sections 2.2 - 4 outline our method for adapting HMC to the overlap operator. Section 5 gives first numerical results, demonstrating how the algorithm works in practice. After a brief conclusion, there are two appendices, proving that our proposed algorithm satisfies detailed balance, and describing the correction update when two eigenvalues cross zero during the same time step.

#### 2 Hybrid Monte Carlo

#### 2.1 HMC for Wilson fermions

This subsection is a short review of the HMC algorithm for the case of Wilson fermions [38].

The standard Wilson Dirac operator on the lattice, with a mass  $-m_0$ , is

$$M_{xy,\alpha\beta,ij} = \delta_{xy}\delta_{\alpha\beta}\delta_{ij} - \kappa \sum_{\mu} \left( \left( 1 - \gamma_{\mu}^{\alpha\beta} \right) U_{\mu}^{ij}(x) \delta_{x+e_{\mu},y} + \left( 1 + \gamma_{\mu}^{\alpha\beta} \right) U_{\mu}^{\dagger ij}(x - e_{\mu}) \delta_{x-e_{\mu},y} \right).$$

$$\kappa = \frac{1}{8 - 2m_{0}}.$$
(1)

The Wilson operator is  $\gamma_5$ -hermitian, implying that one can construct a hermitian Wilson operator

$$Q = \gamma_5 M. \tag{2}$$

The Hybrid Monte-Carlo method updates the gauge field in two steps: (1) a molecular dynamics evolution of the gauge field; (2) a Metropolis step which renders the algorithm exact. In the molecular dynamics step, we introduce a momentum,  $\Pi$ , which is conjugate to the gauge fields U [51]. We introduce a computer time  $\tau$ , and define  $\Pi$  so that

$$dU/d\tau = \dot{U} = i\Pi U. \tag{3}$$

Since U is unitary,  $\Pi$  must be a hermitian traceless matrix. Following the classical equations of motion of this system will generate the correct ensemble. Using the Wilson gauge action, the energy of this system is

$$E(\tau) = \beta \sum_{x} (1 - \frac{1}{2N_C} Tr(U(x)_{\mu\nu} + U(x)_{\mu\nu}^{\dagger})) + X_W^{\dagger} \Phi + \frac{1}{2} \sum_{x} Tr \Pi^2,$$
 (4)

$$X_W = Q^{-2}\Phi. (5)$$

- (1)  $\Pi(\tau + \Delta \tau/2) = \Pi(\tau) + \Delta \tau \dot{\Pi}(\tau)/2$ .
- (2)  $U(\tau + \Delta \tau/2) = e^{i(\Delta \tau/2)\Pi(\tau + \Delta \tau/2)}U(\tau).$ (3)  $U(\tau + \Delta \tau) = e^{i(\Delta \tau/2)\Pi(\tau + \Delta \tau/2)}U(\tau + \Delta \tau/2).$
- (4)  $\Pi(\tau + \Delta \tau) = \Pi(\tau + \Delta \tau/2) + \Delta \tau \dot{\Pi}(\tau + \Delta \tau)/2$ .

#### **Algorithm 1.** The standard leapfrog update.

 $U(x)_{\mu\nu}$  is the plaquette,  $\Phi$  is a Gaussian-random spinor field, and  $N_C$  is the number of colours (in this work, we take  $N_C = 3$ ). The second equation of motion can be inferred from the condition

$$\dot{E} = 0$$

$$= \sum_{x,\mu} \text{Tr} \left[ \frac{1}{2} \frac{d}{d\tau} (\Pi_{\mu}(x)^{2}) - i \left( \frac{\beta}{6} \Pi_{\mu}(x) U_{\mu}(x) V_{\mu}(x) + \Pi_{\mu}(x) F_{\mu}(x) - h.c. \right) \right].$$
(6)

This gives

$$\dot{\Pi}_{\mu}(x) = i \left[ \left( \frac{\beta}{6} U_{\mu}(x) V_{\mu}(x) + F_{\mu}(x) - h.c. \right) \right]_{\text{Traceless}}.$$
 (7)

Here  $V_{\mu}(x)$  is the staple, the sum over all the remaining parts of the plaquettes which contain the specific gauge link  $U_{\mu}(x)$ .  $F_{\mu}(x)$  is the fermionic force, which can be found by differentiating  $X_W^{\dagger}\phi$  with respect to  $U_{\mu}(x)$ . For Wilson fermions, the fermionic force is

$$F_{\mu}(x) = \kappa (MX_W)_{x+e_{\mu}} X_W^{\dagger}(x) (1+\gamma_{\mu}) + X_W(x+e_{\mu}) (MX_W)^{\dagger}(x) (1-\gamma_{\mu}).$$
(8)

The classical equations of motion have to be solved numerically to generate a new configuration. To maintain detailed balance, each molecular dynamics update from computer time  $\tau$  to computer time  $\tau + \Delta \tau$  needs to be area conserving (i.e. the Jacobian for the update is 1), and reversible <sup>3</sup>. The leapfrog algorithm fulfils both these requirements, and, over an entire trajectory, conserves energy up to order  $\Delta \tau^2$ . For later convenience, we will write it in terms of a four step procedure updating the momentum fields and gauge fields in turn (see algorithm 1). The HMC update consists of  $n_{md}$  molecular dynamics steps followed by a Metropolis step to correct for the small violation in energy conservation caused by the numerical integration.

Starting with a configuration  $\{U(0),\Pi(0)\}\$ , we perform a molecular dynamics step to reach a configuration  $\{U(\Delta\tau),\Pi(\Delta\tau)\}$ . If the update is reversible, repeating the molecular dynamics step backwards, with  $\Delta \tau = -\Delta \tau$ , will return to the original configuration.

#### 2.2 Naive HMC with overlap fermions

The overlap operator is given by [18]

$$D = (1 + \mu) + \gamma_5 (1 - \mu) sign(Q), \tag{9}$$

where  $\mu$  is a mass term. The bare fermion mass is

$$m_b = 2\mu m_0/(1-\mu),$$
 (10)

where  $m_0$  is the mass of the Wilson operator Q. The Hermitian overlap operator reads

$$H = \gamma_5 D. \tag{11}$$

The fermion action is thus  $S_{pf} = \phi^{\dagger} H^{-2} \phi$ . We approximate the matrix sign function using a rational approximation. It is frequently advantageous when calculating the sign function to treat the smallest eigenvalues of Q explicitly in a spectral representation. If we project out the lowest  $n_e$  eigenvectors of Q, then the rational fraction, which approximates the sign function for eigenvalues of  $Q^2$  within the fixed range  $[\alpha^2, \beta^2]$ , is modified to read

$$\operatorname{sign}(Q) = aQ \sum_{k} A^{k} \omega_{k}(\alpha, \beta) \left( 1 - \sum_{l=1}^{n_{e}} |\psi^{l}\rangle \langle \psi^{l}| \right) + \sum_{l=1}^{n_{e}} |\psi^{l}\rangle \langle \psi^{l}| \epsilon(\lambda_{l}),$$
 (12)

$$A^k = \frac{1}{a^2 Q^2 + \zeta_k(\alpha, \beta)}. (13)$$

Here  $a=1/\alpha$ ,  $|\psi^l\rangle$  are the eigenvectors of Q with eigenvalue  $\lambda_l$ , and  $\epsilon(\lambda)$  denotes the sign function. We shall assume that  $\omega$  and  $\zeta$ , the coefficients of the rational fraction, are known (here we used the Zolotarev coefficients [52,53]). During the course of the Hybrid Monte Carlo, we should keep the coefficients  $\alpha$  and  $\beta$  fixed to maintain the acceptance rate, which requires the projection of all eigenvectors with eigenvalues below  $\alpha$ .

Of course, we are free to project out eigenvectors within the Zolotarev range as well, either exactly, as in (12), or from the rational approximation itself:

$$\sum_{k} \frac{\omega_{k}}{a^{2}Q^{2} + \zeta_{k}} = \sum_{k} \frac{\omega_{k}}{a^{2}Q^{2} + \zeta_{k}} \left( 1 - \sum_{l=n_{e}+1}^{n_{p}} |\psi^{l}\rangle\langle\psi^{l}| \right) + \sum_{l=n_{e}+1}^{n_{p}} |\psi^{l}\rangle\langle\psi^{l}| \sum_{k} \frac{\omega_{k}}{a^{2}\lambda_{l}^{2} + \zeta_{k}}.$$

$$(14)$$

Our preferred method is to project out a fixed number,  $n_p$ , of eigenvectors, treating the eigenvectors below  $\alpha$  exactly according to (12), and using (14)

for any eigenvectors that lie within the range of the rational fraction approximation. The value of  $\alpha$  is chosen so that most of the time all the eigenvalues of  $Q^2$  lie within the range  $[\alpha^2, \beta^2]$  - only when one of the Wilson eigenvectors crosses the zero axis will we need to project the eigenvalue out of the sign function itself (according to (12)). The reason we proceed in this manner is that we have to perform an additional two inversions of the Wilson operator per fermion flavour for each eigenvalue projected out of the sign function when calculating the fermionic force. This outweighs the gain to be achieved by increasing the parameter  $\alpha$  (although there is some room for optimising its actual value).

In order to calculate the fermionic force we need to differentiate the sign function with respect to computer time, which means that we must differentiate both the rational fraction, and the smallest eigenvalues and eigenvectors. To differentiate the eigenvalues, we start with the eigenvalue equation

$$Q|\psi^l\rangle = \lambda_l|\psi^l\rangle. \tag{15}$$

We now perform an infinitesimal change in the matrix  $Q, Q \to Q + \delta Q$ . The new eigenvalue equation reads

$$(Q + \delta Q) (|\psi^l\rangle + |\delta\rangle) = (\lambda_l + \delta \lambda) (|\psi^l\rangle + |\delta\rangle), \qquad (16)$$

where we are free to define  $|\delta\rangle$  so that  $\langle\psi^l|\delta\rangle=0$ . We immediately have

$$\dot{\lambda}_l = \langle \psi^l | \dot{Q} | \psi^l \rangle \tag{17}$$

$$\frac{d}{d\tau}|\psi^l\rangle = -P_l\dot{Q}|\psi^l\rangle \tag{18}$$

$$P_l = (1 - |\psi^l\rangle\langle\psi^l|)(Q - \lambda_l)^{-1}(1 - |\psi^l\rangle\langle\psi^l|). \tag{19}$$

We have added a second eigenvector projector to (19) so that both  $\langle \phi | P_l$  and  $P_l | \phi \rangle$  can be calculated numerically. We are now in a position to calculate the fermionic force in the usual manner (sums over k, l and repeated spatial indices  $\mu$  and x will be assumed from this point onwards):

$$\dot{U}_{\mu}(x)F_{\mu}(x) + F_{\mu}^{\dagger}(x)\dot{U}_{\mu}^{\dagger}(x) = -(1-\mu^{2})\langle X|\left(\gamma_{5}\frac{d}{d\tau}\operatorname{sign}Q + \frac{d}{d\tau}\operatorname{sign}Q\gamma_{5}\right)|X\rangle,$$
(20)

$$X = H^{-2}\phi. (21)$$

The differential of the sign function is:

$$\left(\frac{d}{d\tau}\operatorname{sign}Q\right)_{nm} = \dot{U}_{\mu}(x)\left(\tilde{F}_{\mu,nm}^{R}(x) + \tilde{F}_{\mu,nm}^{P}(x) + \tilde{F}_{\mu,nm}^{S}(x) + \tilde{F}_{\mu,nm}^{D}(x)\right) + h.c.,$$
(22)

where  $\tilde{F}^R$  is the term generated by differentiating the rational approximation,  $\tilde{F}^P$  is the term generated by differentiating the eigenvector projector  $1 - |\psi^l\rangle\langle\psi^l|$ , while  $\tilde{F}^S$  and  $\tilde{F}^D$  come from the differential of  $\epsilon(\lambda)$  in (12). These four terms are:

$$\tilde{F}_{\mu,nm}^{R}(x) = \kappa a \omega_{\eta} A_{na}^{k} \left[ a^{2} Q_{ax} \gamma_{5} (1 - \gamma_{\mu}) \delta_{x+e_{\mu},c} Q_{cd} \right. \\
\left. - \zeta_{k} \gamma_{5} (1 - \gamma_{\mu}) \delta_{a,x} \delta_{x+e_{\mu},d} \right] A_{de}^{k} \left( 1 - |\psi^{l}\rangle \langle \psi^{l}| \right)_{em}, \\
\tilde{F}_{\mu,nm}^{P}(x) = - \kappa Q A_{na}^{k} P_{l,ax} \gamma_{5} (1 - \gamma_{\mu}) \delta_{x-e_{\mu},c} \left( |\psi^{l}\rangle \langle \psi^{l}| \right)_{cm} \\
\left. - \kappa Q A_{na}^{k} \left( |\psi^{l}\rangle \langle \psi^{l}| \right)_{ax} \gamma_{5} (1 - \gamma_{\mu}) \delta_{x,c+e_{\mu}} P_{l,cm}, \right. \\
\tilde{F}_{\mu,nm}^{S}(x) = \kappa P_{l,nx} \gamma_{5} \epsilon(\lambda_{l}) (1 - \gamma_{\mu}) \delta_{x,c+e_{\mu}} \left( |\psi^{l}\rangle \langle \psi^{l}| \right)_{cm} \\
\left. + \kappa \left( |\psi^{l}\rangle \langle \psi^{l}| \right)_{nx} \gamma_{5} (1 - \gamma_{\mu}) \delta_{x,c+e_{\mu}} \epsilon(\lambda_{l}) P_{l,cm}, \right. \\
\tilde{F}_{\mu,nm}^{D}(x) = - \left( |\psi^{l}\rangle \langle \psi^{l}| \right)_{nm} \frac{d\epsilon(\lambda_{l})}{d\lambda_{l}} \langle \psi^{l}|_{x} \gamma_{5} (1 - \gamma_{\mu}) \delta_{x,c+e_{\mu}} |\psi^{l}\rangle_{c}. \tag{23}$$

For later convenience, we define  $F^G$  as the gauge field force, and  $F^C$  as the continuous part of the fermionic force, i.e.,

$$F_{\mu}^{G}(x) = \langle X | i \frac{\beta}{6} U_{\mu}(x) V_{\mu}(x) | X \rangle + h.c. ,$$

$$F_{\mu}^{C}(x) = -(1 - \mu^{2}) i U_{\mu}(x) \langle X | \left\{ \gamma_{5}, \tilde{F}_{\mu}^{R}(x) + \tilde{F}_{\mu}^{P}(x) + \tilde{F}_{\mu}^{S}(x) \right\} | X \rangle + h.c. .$$
(25)

To calculate the fermionic force, we need to invert the overlap operator twice, perform two multi-mass inversions of the Zolatarev rational function, and, as remarked before, calculate two inversions of the Wilson operator per fermion flavour and eigenvalue projected out of the sign function. This formula can be inserted into a HMC routine for Wilson or staggered fermions. However, the last term in (23) contains a Dirac delta function (the derivative of the sign function) that will ruin the performance of standard integrators. Whenever an eigenvalue of the Wilson operator crosses zero on a HMC trajectory, special attention has to be paid to this last term. We note in passing that eigenvalue crossings of the Wilson operator are associated with a change in the topological charge  $\nu = -\frac{1}{2} \text{Tr}(\text{sign } Q)$ .

#### 3 Eigenvalue Crossings

#### 3.1 Possible strategies

There are at least three approaches which can be taken to overcome the problem of the eigenvalue crossing:

- (1) Ignore the problem altogether in the hope that it will go away with increasing values of  $\beta$ . In this spirit, one would use chiral projection [42] to allow for sampling across different topological sectors, and a small path length to compensate for the low acceptance rate. Though in principle this recipe might allow the simulation to bypass the potential wall, but this method is clearly far from satisfactory. In fact, our studies suggest that at  $\beta = 5.6$  this approach generates an ensemble of "deconfined" configurations.
- (2) Replace  $\epsilon$  with some continuous function for small  $\lambda$  [42]. The substitute of the sign function will have to be broad enough so that the low eigenvalues notice it, but not so broad that it leads to a large deviation in the final Monte Carlo ensemble. In principle, it should be possible to narrow the revised  $\epsilon$  as the time step decreases. One can reduce these artifacts by using a more accurate overlap operator in the accept/reject step than in the molecular dynamics [42], but this will lower the acceptance rate.
- (3) As soon as one encounters a crossing, one jumps back and repeats the micro-canonical step, with the integration over the delta function treated exactly [26,44].

Albeit being more costly (per HMC trajectory) than the first two approaches, method (3) is our strategy of choice as it offers best control over systematic errors from the Dirac delta function's contribution to the fermionic force, as will be explained in the following sections.

#### 3.2 The effect of the crossing

The eigenvalue crossing induces a discontinuity in the fermionic contribution to the action, the kinetic energy, and the fermionic force. The Monte Carlo energy is

$$E = \beta \sum_{x} \left(1 - \frac{1}{2N_C} Tr(U(x)_{\mu\nu} + U(x)_{\mu\nu}^{\dagger})\right) + X^{\dagger} \Phi + \frac{1}{2} \sum_{x} Tr \Pi_{\mu}^{2}(x).$$
 (26)

We want to generate the second equation of motion from energy conservation

$$\frac{dE}{d\tau} = 0 = \dots + \Phi^{\dagger} \frac{d}{d\tau} (H^{-2}) \Phi. \tag{27}$$

Care needs to be taken when differentiating the fermionic contribution to the action near to a singularity in the Wilson operator. We note that for a discontinuous function a, with  $\lim_{\delta\tau\to 0} a(\tau-\delta\tau) \neq \lim_{\delta\tau\to 0} a(\tau+\delta\tau)$ , the differential of the product of a and b is not the usual formula:

$$\frac{d}{d\tau}(ab) = \lim_{\delta\tau \to 0} a(\tau + \delta\tau) \frac{db}{d\tau} \bigg|_{\tau} + b(\tau) \frac{da}{d\tau} \bigg|_{\tau}. \tag{28}$$

 $(da/d\tau|_{\tau})$  will of course be proportional to  $\delta(\tau)$ ). Therefore,

$$\frac{d}{d\tau}H^{-2} = -\lim_{\delta\tau \to 0} H^{-2}(\tau + \delta\tau) \left. \frac{dH^2}{d\tau} \right|_{\tau} H^{-2}(\tau). \tag{29}$$

If there is a discontinuity in H, such as when the eigenvalue  $\lambda_1$  crosses zero, then we need to take one inversion just before the crossing, giving  $X_- = H^{-2}(\lambda_1)\phi$ , and the other inversion just after it, giving  $X_+ = H^{-2}(-\lambda_1)\phi$ :

$$\frac{dE}{d\tau} = 0 = \sum_{x,\mu} \text{Tr} \left[ \frac{1}{2} \frac{d}{d\tau} \Pi_{\mu}^{2}(x) - i \frac{\beta}{6} \left( \Pi_{\mu}(x) U_{\mu}(x) V_{\mu}(x) - h.c \right) + (1 - \mu^{2}) \langle X_{+} | \left( \gamma_{5} \frac{d}{d\tau} \text{sign} Q + \frac{d}{d\tau} \text{sign} Q \gamma_{5} \right) | X_{-} \rangle \right].$$
(30)

Let us denote the momenta just before and after the eigenvalue crossing as  $\Pi^-$  and  $\Pi^+$  respectively (with the smallest eigenvalues  $\lambda_-$  and  $\lambda_+$ ). We can recast equation (30) into the form

$$\frac{1}{2\delta\tau} \left[ (\Pi^{+})^{2} - (\Pi^{-})^{2} \right] = -(1-\mu^{2})\langle X_{+}| \left( \gamma_{5} |\psi^{l}\rangle \langle \psi^{l}| + |\psi^{l}\rangle \langle \psi^{l}| \gamma_{5} \right) |X_{-}\rangle \frac{\epsilon(\lambda_{-}) - \epsilon(\lambda_{+})}{\delta\tau}.$$
(31)

This shows that integrating over the Dirac  $\delta$  function in the fermionic force will produce a discontinuity in the kinetic energy:

$$(\Pi^{+})^{2} - (\Pi^{-})^{2} = 4d(\tau_{c})$$

$$d(\tau) = -(1 - \mu^{2})\epsilon(\lambda_{-})\langle X_{+}(\tau)|\gamma_{5}|\psi^{l}(\tau)\rangle\langle\psi^{l}(\tau)|X_{-}(\tau)\rangle$$

$$-(1 - \mu^{2})\epsilon(\lambda_{-})\langle X_{+}(\tau)|\psi^{l}(\tau)\rangle\langle\psi^{l}(\tau)|\gamma_{5}|X_{-}(\tau)\rangle.$$

$$(32)$$

It is easy to show that this discontinuity in the kinetic energy will exactly cancel the discontinuity in the pseudo-fermion action  $\langle X_+|\Phi\rangle - \langle X_-|\Phi\rangle$ . Therefore, energy is conserved across the eigenvalue crossing in an exact integration. Our task is now to develop an integration algorithm such as to maintain area conservation, energy conservation and reversibility in the presence of Dirac delta function forces.

### 4 HMC with overlap fermions

#### 4.1 The algorithm

We propose to add a correction step to the *standard leapfrog* algorithm (algorithm 1) to handle the above discontinuities from eigenvalue crossing. This

correction step has to be area preserving, reversible, and ideally should satisfy (30) with  $O(\Delta \tau^2)$  errors or better to comply with the standard integration procedure. We shall develop the appropriate integrator on the interval of crossing by an explicit construction.

In this section we shall first outline the method by which suitable correction steps can be derived; after that, we shall present our integrator of choice, leaving the proof that its correction step is area conserving, reversible and conserves energy with only  $O(\Delta \tau^2)$  errors to appendix A.

First, let us specify some notation: We operate on a 4 dimensional space time lattice with V lattice sites and 4V links. We deal with the  $SU(N_C)$  gauge group (for most of this work we shall set  $N_C=3$ ), so the gauge field is  $U_\tau$  contains a member of  $SU(N_C)$  on every link, and the momentum field  $\Pi_\tau$  is represented by a Hermitian, traceless  $N_C \times N_C$  matrix on each link. The subscript  $\tau$  refers to the computer time at which the gauge or momentum field is calculated. For convenience, we shall set  $\Delta \tau = 1$ , and assume that we start at time 0, so that  $U_0$  is the original gauge field, and  $U_1$  the final gauge field at the end of the leapfrog correction step.  $\tau_c + 1/2$  is the computer time at which the eigenvalue is 0 (we shall discuss how to calculate  $\tau_c$  at the end of this section). We shall use the superscript "—" to indicate that we have not yet included the effects of the crossing into the momentum update, and "+" to indicate that the momentum has been updated to account for the crossing. We shall write  $\Pi^+ \equiv \Pi_{\frac{1}{2}}^+$  etc., and  $U_c \equiv U_{\frac{1}{2}+\tau_c}^- = U_{\frac{1}{2}+\tau_c}^+$ . Finally, the notation (A, B) shall be used to represent  $\sum_{x,\mu} \text{Tr}(A_\mu(x)B_\mu(x))$ . The continuous part of the (hermitian) force is  $F_\tau = F_\tau^G + F_\tau^C$ , with  $F^G$  and  $F^C$  defined in equations (24) and (25).

U contains an element of  $SU(N_C)$  for every link, while  $\Pi$  is a generator of U, i.e. it contains a hermitian, traceless  $N_C \times N_C$  matrix on every link. To simplify the notation at a later stage in the argument, we expand  $\Pi$  in terms of an orthonormal basis defined by a set of orthonomal basis vectors which we divide into  $N_S$  subsets,  $\{\{\eta_1^1, \eta_2^1, \ldots\}, \{\eta_1^2, \eta_2^2, \ldots\}, \ldots\}$  and the parameter  $N_k$  gives the number of  $\eta$  vectors in each subset k. The  $\eta_i^k$  are  $4V(N_C^2 - 1)$  hermitian traceless matrices which satisfy  $(\eta_i^k, \eta_j^m) = \delta_{ij}\delta^{km}$ .  $N_k$  and  $N_S$  are defined so that the subscripts (i and j) run from 1 to  $N_k$ , where  $N_k$  is not necessarily constant for all the k, while the superscripts (k and m) run from 1 to  $N_S$ . For the moment, we shall leave the  $N_k$ s and  $N_S$  as arbitary parameters, which satisfy the constraint

$$\sum_{k=1}^{N_S} N_k = 4V(N_C^2 - 1).$$

The basis is thus complete, so that

$$\Pi = \sum_{k=1}^{N_S} \sum_{k=1}^{N_k} \eta_i^k (\eta_i^k, \Pi).$$
 (34)

The  $\eta$  matrices should just be functions of  $U_c$ , and are otherwise independent of the momentum. We will define  $\eta_1^1 \equiv \eta$  as being normal to the gauge field surface where the eigenvalue is zero (see appendix A and equation (A.29)).  $\eta_2^1$  is proportional to  $F - \eta(\eta, F)$ , where  $F = F_{\tau_c+1/2}^+ - F_{\tau_c+1/2}^-$ . The other  $\eta$  matrices are arbitrary.

Having defined our notation, we can now proceed to construct the correction update,  $(\Pi_0, U_0) \to (\Pi_1, U_1)$ . The first step is to update the gauge and momentum to time  $\tau + \Delta \tau/2$ , as in the leapfrog procedure (algorithm 1), to yield fields  $\Pi^-$  and  $U^-$ :

$$\Pi^{-} = \Pi_{0} + (F_{0}^{-}) \frac{\Delta \tau}{2} 
U^{-} = e^{i\Delta \tau \Pi_{-}/2} U_{0}.$$
(35)

Next, we need to integrate up to the crossing point itself:

$$\Pi_{\frac{1}{2} + \tau_c}^- = \Pi^- + \tau_c F^- \tag{36}$$

$$U_c = e^{i\tau_c \Pi^-} U^-. \tag{37}$$

We now perform the correction step. Equation (32) reads:

$$\left(\Pi_{\frac{1}{2}+\tau_c}^+, \Pi_{\frac{1}{2}+\tau_c}^+\right) = \left(\Pi_{\frac{1}{2}+\tau_c}^-, \Pi_{\frac{1}{2}+\tau_c}^-\right) + 4d. \tag{38}$$

In terms of our basis, a general solution of (38) is

$$\Pi_{\frac{1}{2}+\tau_{c}}^{+} = \Pi_{\frac{1}{2}+\tau_{c}}^{-} + \sum_{k=1}^{N_{S}} \left( \sum_{i=1}^{N_{k}} \eta_{i}^{k} (\eta_{i}^{k}, \Pi_{\frac{1}{2}+\tau_{c}}^{-}) \right) \left( \sqrt{1 + \frac{d_{k}}{\sum_{i} (\eta_{i}^{k}, \Pi_{\frac{1}{2}+\tau_{c}}^{-})^{2}}} - 1 \right),$$

$$\sum_{i} d_{k} = 4d. \tag{39}$$

Finally, we move back to computer time  $\tau + \Delta \tau/2$ , and complete the rest of the normal leapfrog integration

$$\Pi^{+} = \Pi_{\frac{1}{2} + \tau_{c}}^{+} - \tau_{c} (F_{+}) \tag{40}$$

$$U^+ = e^{-i\tau_c\Pi^+}U_c$$

$$U_1 = e^{i\Delta\tau/2\Pi^+} U^+$$

$$\Pi_1 = \Pi^+ + F_1^+ \frac{\Delta \tau}{2}.\tag{41}$$

This is the naive update algorithm; unfortunately we cannot use it for two reasons: firstly, there is the possibility that one of the square roots in equation (39) might be imaginary; and secondly because the steps described in equations (36) and (40) violate detailed balance. Although  $\tau_c$  is a function of the momentum, this alone is not enough to violate detailed balance, but, as shown in appendix A, an update to the momentum parallel to  $\eta$  will violate area conservation. To satisfy detailed balance, we can update the momentum in directions normal to  $\eta$ , i.e. we replace (36) and (40) by  $\Pi_{1/2+\tau_c}^{\pm} = \Pi^{\pm} + \tau_c(F^{\pm} - \eta(\eta, F^{\pm}))$ ; however, this replacement comes at the cost of an  $O(\tau_c)$  violation of energy conservation. In appendix A, we shall show that a general momentum integration step which satisfies detailed balance is

$$\Pi^{+} = \Pi^{-} + \tau_{c}(F - \eta(\eta, F)) - \frac{\tau_{c}}{3} \operatorname{Tr} F + \eta(\eta, \Pi^{-}) \left( \sqrt{1 + \frac{d_{1}}{(\eta, \Pi^{-})^{2}}} - 1 \right) + \sum_{k=2}^{N_{S}} \left[ \eta_{1}^{k}(\eta_{1}^{k}, \Pi^{-} - \frac{\tau_{c}}{2}(F^{+} + F^{-})) + \eta_{2}^{k}(\eta_{2}^{k}, \Pi^{-} - \frac{\tau_{c}}{2}(F^{+} + F^{-})) \right] \times \left[ \sqrt{1 + \frac{d_{1}}{[\eta_{1}^{k}, \Pi^{-} - \frac{\tau_{c}}{2}(F^{+} + F^{-})]^{2} + [\eta_{2}^{k}, \Pi^{-} - \frac{\tau_{c}}{2}(F^{+} + F^{-})]^{2}} - 1 \right].$$
(42)

We have inserted the fermionic force dependence here for later convenience. To satisfy detailed balance, we need  $N_k = 2 \ \forall k$ , and the  $d_k$  should be functions only of the gauge field at the crossing and (for  $k \neq 1$ )  $(\eta, \Pi^-)$ , and odd functions of  $\Delta \tau$ . If we set  $d_1 = 4d$ , and  $d_k = 0 \ \forall k \neq 1$ , then we get an algorithm similar to that proposed in [26,44], which has an  $O(\tau_c)$  energy conservation violating term (see appendix A.3):  $\Delta E = \tau_c((F^+, \eta)(\Pi^-, \eta) - (F^-, \eta)(\Pi^-, \eta))$ . However, we can reduce the errors to  $O(\Delta \tau^2)$  and even remove some of the  $O(\Delta \tau^2)$  errors by simply exploiting one of the other  $d_k$ .

The next problem which we have to face is what to do when one of the square roots in equation (42) is imaginary. We use the solution proposed in [26,44]: reflection of the  $\lambda=0$  surface. A useful analogy is that of a classical mechanics particle approaching a potential wall. If the momentum of the particle normal to the surface of the wall is large enough, then it will pass through the wall, albeit with a changed momentum (i.e.  $(\Pi^+, \eta_1) = \sqrt{(\Pi^-, \eta_1)^2 + 4d}$ , where the kinetic energy of the particle is reduced by 2d.). We call this case transmission, <sup>4</sup> and this is the scenario described so far in this section. If the momentum is too small, the particle will bounce (elastically) off the surface of the potential wall (i.e.  $(\Pi^+, \eta) = -(\Pi^-, \eta)$ ). We call this case reflection. Unlike transmission, a reflection update is accompanied neither with a change in topological charge nor with a discontinuity in the fermionic action.

 $<sup>^4</sup>$  it is called *refraction* in [26,44]

There is one further subtlety which needs to be addressed before we can write down our algorithms for transmission and reflection. The combined update step must also be area conserving (see appendix A.2.3). As an example, suppose that we set  $d_1 = 4d$ , and all the other  $d_k = 0$ , and we reflect whenever  $1 + \frac{4d}{(\eta,\Pi^-)^2} < 0$ . We can then write

$$\Pi^{+} = \Pi^{+\text{transmission}} \theta \left( 1 + \frac{4d}{(\eta, \Pi^{-})^{2}} \right) + \Pi^{+\text{reflection}} \left( 1 - \theta \left( 1 + \frac{4d}{(\eta, \Pi^{-})^{2}} \right) \right). \tag{43}$$

When calculating the Jacobian we must differentiate the  $\theta$  (step) functions, which, unless we take care, would lead to a Jacobian of the form  $1 - \delta(1 +$  $4d/(\eta,\Pi^{-})^{2}$ ). As we argue in appendix A.2.3, this might lead to a small but non-zero systematic error in the final ensemble. Although we have not observed any effect of this violation of detailed balance in our numerical results, we feel that it is safer to avoid the impact of this delta function in the Jacobian. To this end, we reflect only if  $|d| > d_{\text{max}}$ . When  $|d| < d_{\text{max}}$  and  $1 + d_k / \sum_i (\eta_i^k, \Pi^-)^2 < 0$ , for the area conservation we need an update which is real and continuous, and it is impossible to satisfy these conditions and energy conservation simultaneously. We therefore have to compensate on energy conservation when  $d_k$  drops below  $1 + d_k / \sum_i (\eta_i^k, \Pi^-)^2 = 0$ . The parameter  $d_{\text{max}}$ should therefore be carefully tuned: too small, and there will be few eigenvalue crossings, and therefore few changes of the topological charge; too large, and there will be frequent energy conservation violations, leading to a small acceptance rate. We used  $d_{\text{max}} = 0.25$  in our numerical work (although this is not the optimal value), except while checking the independence of various observables on  $d_{max}$ .

#### 4.1.1 Transmission

Our proposed update for transmission is (see algorithm 2)

$$\Pi^{+} = \Pi^{-} + \tau_{c}(F) - \eta \tau_{c}(\eta, F) - \frac{\tau_{c}}{3} \operatorname{Tr}(F) + s_{1}^{1} \sqrt{1 + \frac{4d}{(\eta, \Pi^{-})^{2}}} + \left( \eta_{1}^{2} (\eta_{1}^{2}, \Pi^{-} - \frac{\tau_{c}}{2} (F^{-} + F^{+})) + \eta_{2}^{2} (\eta_{2}^{2}, \Pi^{-} - \frac{\tau_{c}}{2} (F^{-} + F^{+})) \right) \times \left( \sqrt{1 + \frac{d_{2}}{(\eta_{1}^{2}, \Pi^{-} - \frac{\tau_{c}}{2} (F^{-} + F^{+}))^{2} + (\eta_{2}^{2}, \Pi^{-} - \frac{\tau_{c}}{2} (F^{-} + F^{+}))^{2}} - 1 \right) (44)$$

$$s_{1}^{1} = \operatorname{sign} \left( 1 + \frac{4d}{(\eta, \Pi^{-})^{2}} \right),$$

$$d_{2} = -2\tau_{c}(F^{-}, \eta)(\Pi^{-}, \eta) + 2\tau_{c}(F^{+}, \eta)(\Pi^{+}, \eta) + \tau_{c}^{2}(F^{-} + F^{+}, F^{+} - F^{-}).$$

As mentioned earlier,  $\eta_1^2$ , and  $\eta_2^2$  should be orthonormal, and orthogonal to  $\eta$  and F. We construct these vectors from the normals to the constant eigenvalue surfaces of the largest two calculated eigenvectors, but it is likely that better options exist. d,  $F_{\pm}$ ,  $\eta$ ,  $\eta_1^2$ , and  $\eta_2^2$  should only be functions of  $U_c$ , and otherwise independent of the momentum.

A (usually) good first approximation of  $\tau_c$  can be derived from the Taylor expansion of the eigenvalue around zero (see equation (17)):

$$\tau_c = -\frac{\langle \psi^l | Q | \psi^l \rangle}{\langle \psi^l | \dot{Q} | \psi^l \rangle}.$$
 (45)

This gives the correct value of  $\tau_c$  up to order  $\tau_c^2$ . We can in principle calculate  $\tau_c$  using (45) from either the gauge field  $U^+$  or the gauge field  $U^-$ . There will be a small deviation between the two calculations, and therefore a small discrepancy between d and  $\eta$  calculated from the two gauge fields. This will lead to a breakdown in reversibility if we apply the algorithm 2 naively. There are two possible ways in which this problem can be overcome. Firstly, one can calculate  $\tau_c$  from  $U^-$  if  $\tau_c/\Delta\tau < 0$  (i.e. we have already passed the crossing at molecular dynamics time  $\tau + \Delta\tau/2$ ), and use  $U^+$  to calculate  $\tau_c$  otherwise. Calculating  $\tau_c$  using  $U^+$  requires an iterative procedure; we used a combination of simple iteration and the Van Wijngaarden-Dekker-Brent method [54,55] for root finding, which was reasonably effective. The second, and our preferred, possibility is to calculate  $\tau_c$  exactly using a root finding method, such as either Newton-Raphson or the Van Wijngaarden-Dekker-Brent method. We used a Newton-Raphson method, iterating

$$\tau_c^n = \tau_c^{n-1} - \frac{\langle \psi^l(\Delta \tau/2 + \tau_c^{n-1}) | Q | \psi^l(\Delta \tau/2 + \tau_c^{n-1}) \rangle}{\langle \psi^l(\Delta \tau/2 + \tau_c^{n-1}) | \dot{Q} | \psi^l(\Delta \tau/2 + \tau_c^{n-1}) \rangle},\tag{46}$$

so that we could improve the accuracy of the eigenvector as the Newton-Raphson iteration progressed. Trying to restrict the eigenvector between two bounds could lead to the eigenvector escaping from the bounds as the accuracy of the calculation increased. This method has the advantage that it removes one source of  $O(\Delta \tau^2)$  energy conservation violating terms, and it also was faster than the simple iterative method on our small trial lattices. However, the smallest eigenvector needs to be calculated to a very high accuracy <sup>5</sup>.

<sup>&</sup>lt;sup>5</sup> we used the PARPACK Arnoldi algorithm [56,57] after the first Newton-Raphson iteration to get an estimate of the eigenvalue spectrum at  $\tau_c$ , and a CG minimisation of the Ritz functional with intermediate diagonalisation [58] for fine tuning on later iterations

- (1)  $\Pi^{-}(\tau + \Delta \tau/2) = \Pi(\tau) + \Delta \tau/2\dot{\Pi}(\tau);$ (2)  $U^{-}(\tau + \Delta \tau/2) = e^{i(\Delta \tau/2)\Pi^{-}(\tau + \Delta \tau/2)}U(\tau);$
- (3)  $U_c = e^{i\tau_c \Pi^-} U^-;$
- (4) The momentum update given in equation 44 for transmission, or equation (47) for reflection:
- (5)  $U^{+} = e^{-i\tau_c\Pi^{+}}U_c;$ (6)  $U(\tau + \Delta\tau) = e^{i(\Delta\tau/2)\Pi^{+}(\tau + \Delta\tau/2)}U^{+}(\tau + \Delta\tau/2);$
- (7)  $\Pi(\tau + \Delta \tau) = \Pi^+(\tau + \Delta \tau/2) + \Delta \tau/2\dot{\Pi}_+(\tau + \Delta \tau)$

**Algorithm 2.** The modified leapfrog algorithm.

#### 4.1.2 Reflection

The momentum update for reflection (see algorithm 2), used when  $|d| > d_{\text{max}}$ ,

$$\Pi^{+} = \Pi^{-} - 2\eta(\eta, \Pi^{-}) - \left(\eta_{1}^{2}(\eta_{1}^{2}, \Pi^{-} - \tau_{c}F^{-}) + \eta_{2}^{2}(\eta_{2}^{2}, \Pi^{-} - \tau_{c}F^{-})\right) 
+ \left(\eta_{2}^{2}(\eta_{2}^{2}, \Pi^{-} - \tau_{c}F^{-}) + \eta_{1}^{2}(\eta_{1}^{2}, \Pi^{-} - \tau_{c}F^{-})\right) \times 
\left(\sqrt{1 + \frac{d_{2}^{R}}{(\eta_{1}^{2}, \Pi^{-} - \tau_{c}F^{-})^{2} + (\eta_{2}^{2}, \Pi^{-} - \tau_{c}F^{-})^{2}}} - 1\right),$$

$$d_{2}^{R} = 4\tau_{c}(F^{-}, \eta)(\Pi^{-}, \eta).$$
(47)

Note that  $F^+ = F^-$ , since after reflection, the smallest eigenvalue does not change sign.

The sign of the smallest eigenvalue should change for a transmission step, and remain the same for reflection. However on a few rare occasions, this did not occur. Such odd phenomena happen if the  $\lambda = 0$  surface is not smooth near to the point of crossing, so that the eigenvalue might try to cross again in the same molecular dynamics step. We corrected for this by adding a second correction step (i.e. we repeated steps (3) (4) and (5)) if the sign of the smallest eigenvalue did not behave as expected

Two different eigenvalues crossing during the same micro-canonical step will also cause this algorithm to break down, because of possible mixing between the two eigenvectors. This issue will be discussed in appendix B.

#### 5 **Numerical Results**

In this section, we shall test the overlap HMC algorithm numerically on various small lattices. We generated  $4^4$ ,  $N_F = 2$  ensembles with  $\beta = 5.4$ , one set of runs with parameter settings  $\kappa = 0.225$  and  $\mu = 0.05, 0.1, 0.2, 0.3, 0.4$  and 0.5, the other with  $\mu = 0.5$  and  $\kappa = 0.18, 0.19, 0.2, 0.21, 0.22$  and 0.23. We

have also generated three  $6^4$ ,  $\beta = 5.6$  ensembles, with  $\kappa = 0.2$  and  $\mu = 0.3, 0.1, 0.05$ , and two  $8^4$   $\beta = 5.6$  ensembles at at  $\kappa = 0.2$ , and  $\mu = 0.1$  or 0.3, although we did not analyse the small statistics  $8^4$  data sets for most of the results presented in this section. Recent phenomenological calculations using the overlap operator in the quenched approximation have covered masses in the range  $\mu \sim 0.007 \rightarrow 0.4$  [24] or  $\mu \sim 0.015 \rightarrow 0.037$  [59], roughly a factor of 10 below our present mass range <sup>6</sup>. Throughout these simulations, we took advantage of relaxation and preconditioning techniques developed in [48,47]. The accuracy of the preconditioner and number of projected eigenvalues were optimised by our HMC program, which gave gains of  $\sim 30\%$ .

#### 5.1 Energy conservation and topological charge

#### 5.1.1 The correction step and the number of topological charge changes

Our first concern is to verify the impact of the correction step on energy conservation, i.e. on the level of energy fluctuations during a Monte Carlo run. This can be achieved by a comparison of the upper plots of figures 1 and 2, which display the energy variations during the individual trajectories for a typical run. The lower plots in these figures exhibit the tunnelling histories of the systems through the topological sectors. A large spike in the energy difference signals a breakdown in energy conservation. Without the correction step (figure 1) there are spikes in the energy difference whenever the topological charge changes — which occurs when there is an eigenvalue crossing. This confirms our expectation that energy is not conserved when the topological charge changes if the standard leapfrog algorithm is used. In figure 2, we present the same plot, but using the corrected update; generally we find that most of the spikes disappear. The remaining ones can be classified into two categories: (1) A few tunnellings with  $s_1^1 = -1$  in the update equation (44); and (2) some "double spikes," where a large jump in the energy difference is followed by another jump of similar magnitude, but with the opposite sign. This occurs when a positive and a negative eigenvalue of Q both approach, but do not cross, 0 simultaneously. This can cause large mixing between the two eigenvectors. This second effect will not affect the acceptance rate. It should be noted that sometimes the topological charge bounces back within the same time step, which can cause a small discontinuity in the energy (unless, like our code, the HMC algorithm is designed to pick up this possibility).

<sup>&</sup>lt;sup>6</sup> In order to (roughly) express  $\mu$  as a physical mass, we used  $r_0$  to calculate the lattice spacing as approximately  $a^{-1} \sim 590 MeV$  on our  $6^4$  lattices. The renormalisation constant was impossible to measure on these lattices because the error was too large, so, for this rough estimate, we will take  $Z_m = 1$ . This implies that on these ensembles that a quark mass of  $\mu = 0.05$  corresponds to a physical mass of  $\sim 93 MeV$  (with a very large error), i.e. around the value of the strange quark mass.

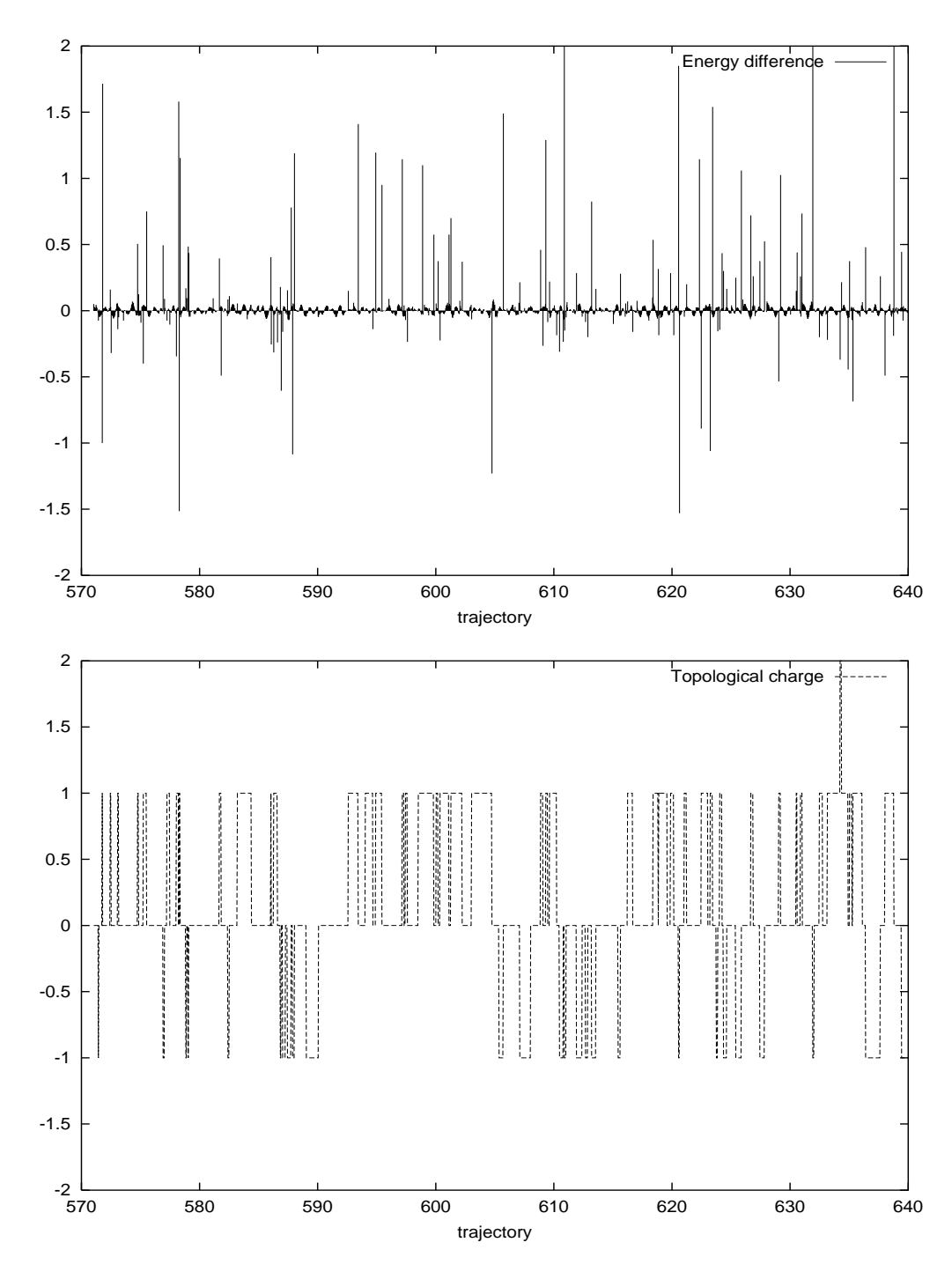


Fig. 1. The energy difference between two micro-canonical steps, and the topological charge plotted against the trajectory number for a  $\beta=5.4,~\mu=0.5,~\kappa=0.225$  ensemble, generated without the correction step.

When we go down to smaller masses, a slightly different picture emerges (see figure 3). We notice that the topological charge changes considerably less frequently at a lower mass (see table 1, 2nd-4th columns), as we would expect — the  $Q \neq 0$  configurations are suppressed as we move to lower masses, and as

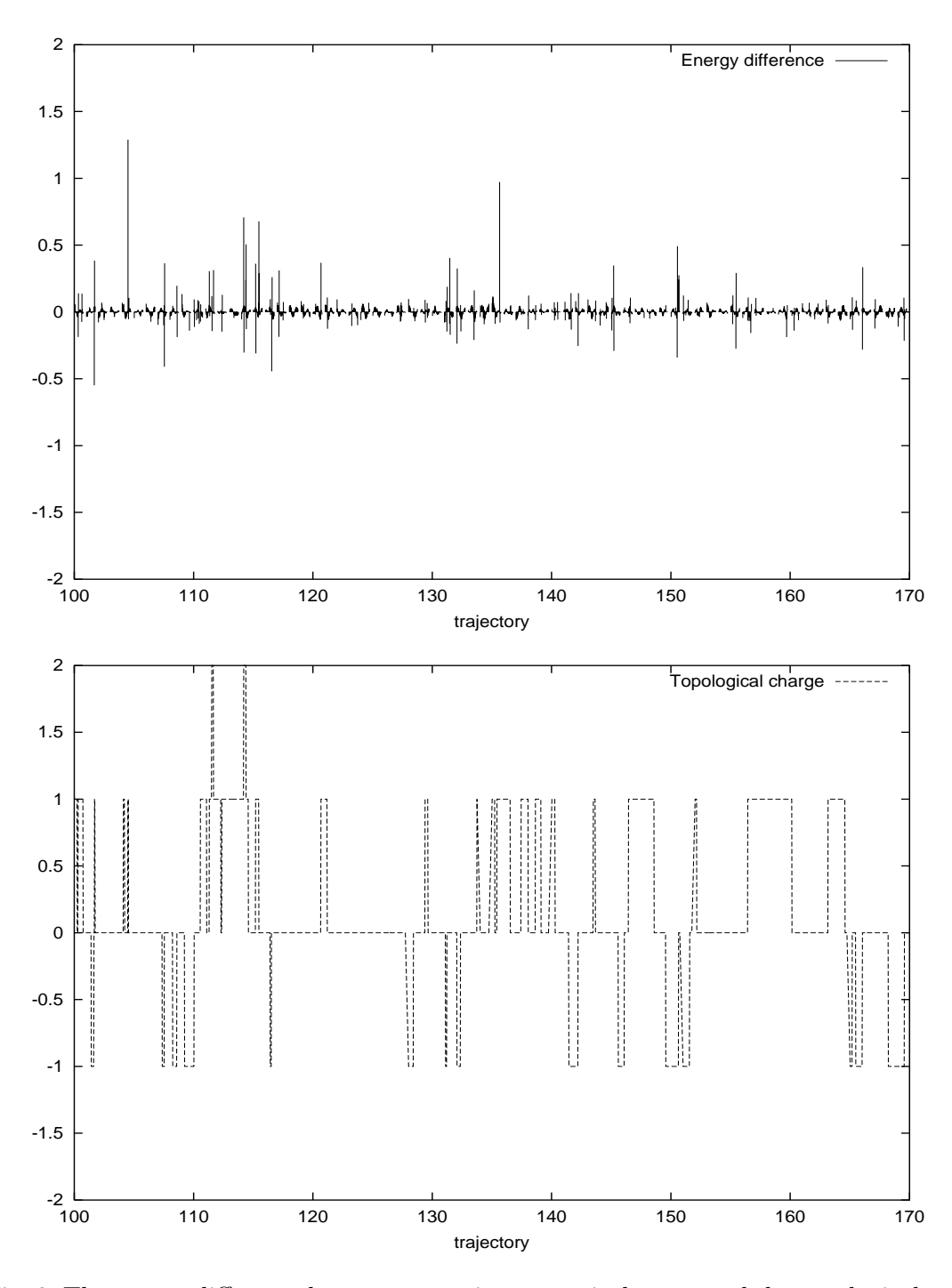


Fig. 2. The energy difference between two micro-canonical steps, and the topological charge plotted against the trajectory number for 70 trajectories of the  $\beta=5.4$ ,  $\mu=0.5$ ,  $\kappa=0.225$  ensemble generated with the correction step.

the mass decreases, d increases, leading to a lower probability of transmission. The energy difference depends strongly on the topological charge (on the  $4^4$ ,  $\mu = 0.05$  ensembles, the mass is about the same size as the lowest non-zero eigenvalue, implying that the inverse of the overlap operator, and therefore

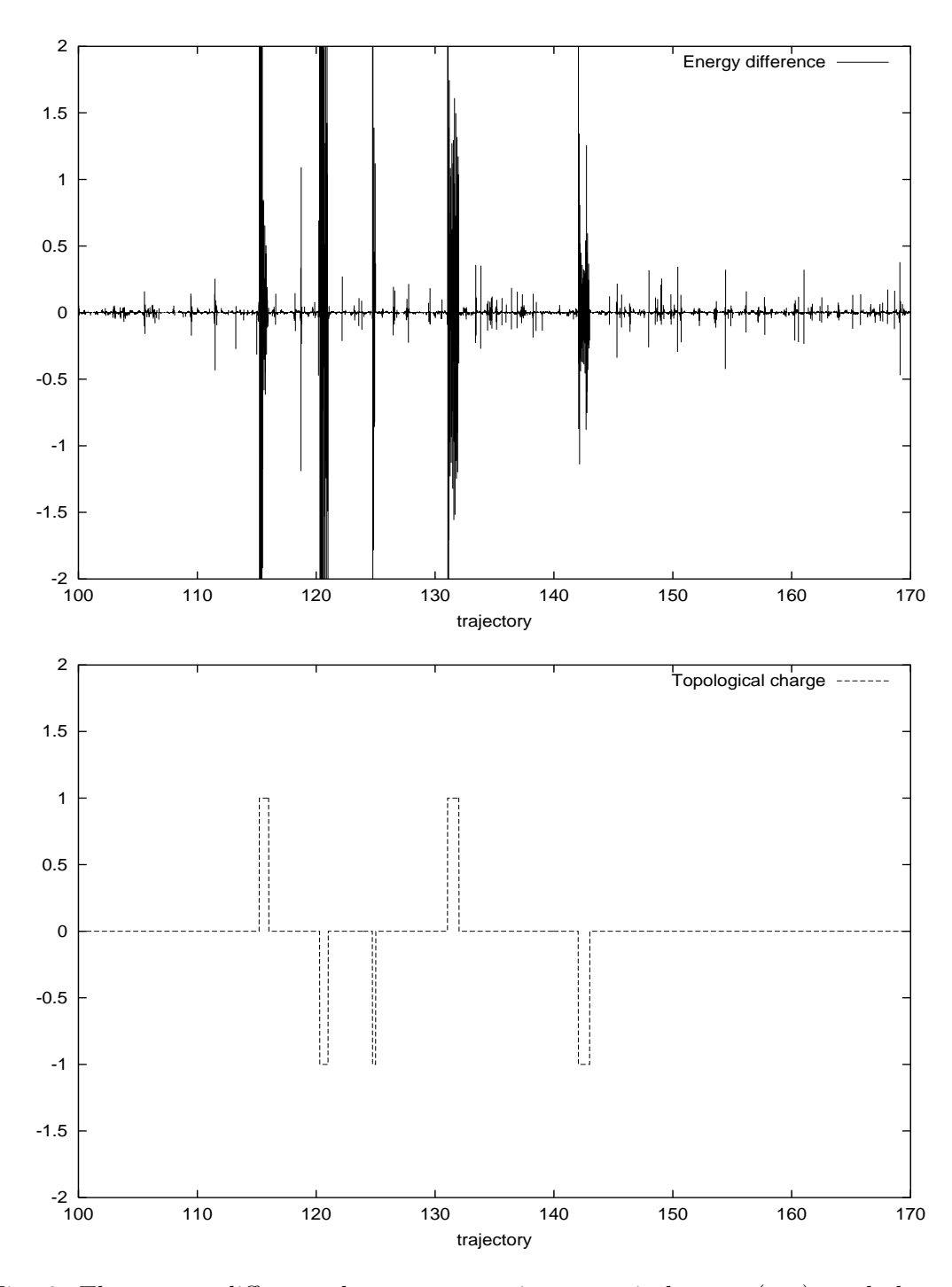


Fig. 3. The energy difference between two micro-canonical steps (top), and the topological charge (bottom) plotted against the trajectory number for 70 trajectories of the  $\beta=5.4~\mu=0.05~\kappa=0.225$  ensemble.

in general the fermionic force, will be larger for a  $Q_f \neq 0$  configuration). This suggests that as we move to even smaller (and more realistic) masses, the update will be very resistant to topological charge changes, because the probability of accepting a configuration with non-zero topological charge will

$4^4$	$\mu = 0.5$	$4^4$	$\kappa = 0.225$	$6^4$	$\kappa = 0.2$	$8^{4}$	$\kappa = 0.2$
$\kappa$	$n_{\mathrm{top}}$	$\mu$	$n_{\mathrm{top}}$	$\mu$	$n_{\mathrm{top}}$	$\mu$	$n_{\mathrm{top}}$
0.18	0.000(0)	0.05	0.045(12)	0.05	0.040(14)		
0.19	0.006(6)	0.1	0.103(20)	0.1	0.074(18)	0.1	0.153(42)
0.2	0.122(31)	0.2	0.393(39)				
0.21	0.579(30)	0.3	0.567(46)	0.3	0.547(74)	0.3	0.969(175)
0.22	0.901(104)	0.4	0.827(52)				
0.23	1.21(83)	0.5	1.12(73)				

Table 1

The number of topological charge changes per trajectory  $(n_{\rm top})$  for various masses on our  $4^4$ ,  $\kappa=0.225$  ensembles (left), the  $4^4$ ,  $\mu=0.5$  ensembles (middle), and the  $6^4$ ,  $\kappa=0.2$  ensembles (right). Note that the  $4^4$  and  $6^4$  ensembles were generated at different values of  $\kappa$  (and  $\beta$ ), so the bare quark mass at constant  $\mu$  is 20% lower for the  $6^4$  ensembles.

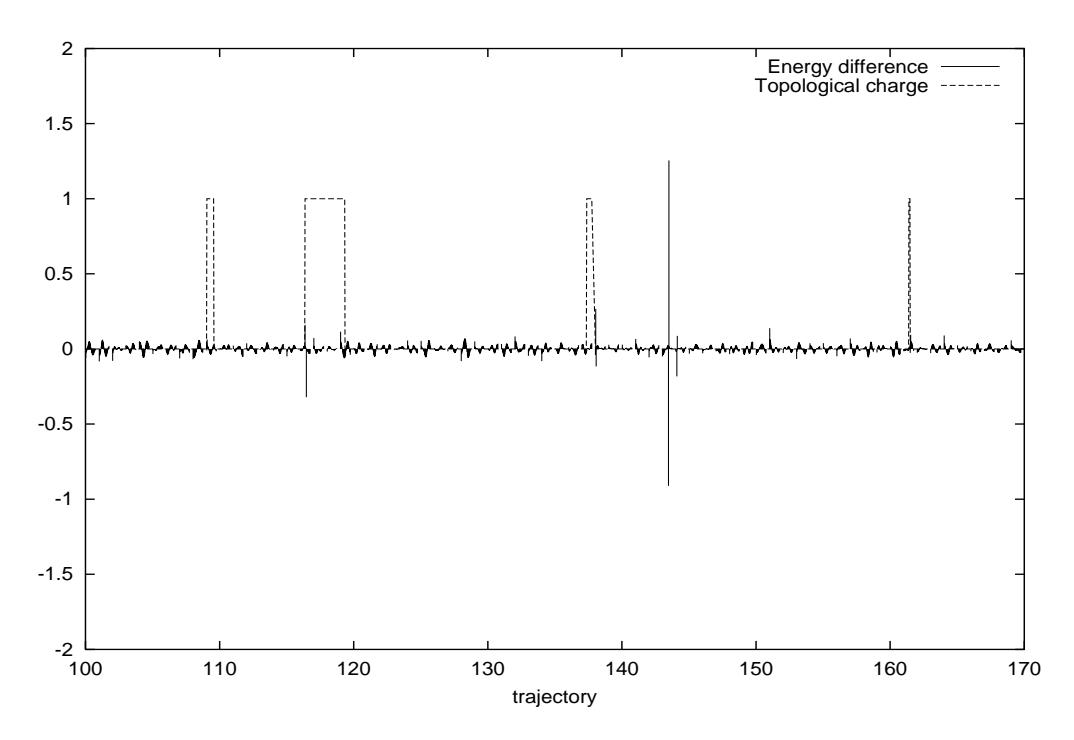


Fig. 4. The energy difference between two micro-canonical steps, and the topological charge plotted against the trajectory number for a section of the  $\beta=5.4~\mu=0.5~\kappa=0.2$ .

become very small as we move to smaller masses. We believe that the method of chiral projection [42] will eliminate this effect. It will help to work on larger lattices, where the overlap operator will be enriched with low eigenvalues. But the nuisance will reappear when the mass is of comparable size to the smallest (non-zero) eigenvalue of the overlap operator.

			[26]			section 4.1			
$n_t$	$1/n_t$	$1/n_t^2$	$ \Delta E_0 $	$\frac{\Delta E_0}{\Delta E_0(n_t=1)}$	$\Delta \tau \frac{\Delta E_0}{\tau_c}$	$ \Delta E $	$\frac{\Delta E}{\Delta E(n_t=1)}$	$\Delta \tau \frac{\Delta E}{\tau_c}$	
1	1.000	1.000	0.120(21)	1.000(172)	0.50(9)	0.059(6)	1.000(105)	0.83(33)	
2	0.500	0.250	0.050(9)	0.414(76)	0.37(5)	0.009(1)	0.154(25)	0.14(4)	
3	0.333	0.111	0.031(7)	0.261(57)	0.32(5)	0.0030(7)	0.051(12)	0.16(8)	
4	0.250	0.063	0.019(4)	0.154(32)	0.31(4)	0.0016(4)	0.027(7)	0.21(14)	
5	0.200	0.040	0.015(3)	0.122(27)	0.31(5)	0.0009(2)	0.015(3)	0.032(8)	
6	0.167	0.028	0.013(3)	0.107(27)	0.35(6)	0.0005(1)	0.008(2)	0.018(4)	
7	0.143	0.020	0.011(2)	0.090(19)	0.34(5)	0.0004(1)	0.007(2)	0.019(4)	

Table 2

The energy difference  $\Delta E$  for the transmission correction algorithm 2 compared with the molecular dynamics time step,  $\Delta \tau = 1/(30n_t)$ . For comparison, results for the algorithm given in [26],  $\Delta E_0$ , are also included.

Finally, it can be seen that reducing  $\kappa$  (and therefore reducing the Wilson mass  $m_0$  and as a consequence the bare fermion mass) generally reduces the number of crossings (see figure 4 and table 1 (first column)). As expected [60,61], there are no changes in the topological charge below the critical value of  $\kappa$ , which is around 0.2 on the  $4^4$  lattices. We confirm that the overlap operator has very few small eigenvalues below the critical value of  $\kappa$  [62].

#### 5.1.2 The size of the error for the correction step

To investigate the  $\Delta \tau$  dependence of the energy conservation violation for the correction step, we took 100 6<sup>4</sup>,  $\mu = 0.3$  configurations, containing 35 transmission correction steps and 123 reflection correction steps. We ran the molecular dynamics as normal (with  $\Delta \tau = 1/30$ ) up to the eigenvalue crossing. We then reduced the time step for the molecular dynamics to  $\Delta \tau/n_t$ , running  $n_t - 1$  normal leapfrog updates and one modified leapfrog update. We calculated the (absolute value of the) error in the energy for the modified leapfrog step only, and averaged over the configurations. This procedure ensures that on each configuration the gauge field and momentum at the crossing have only a small dependence on  $n_t$ . The energy differences for our procedures (algorithm 2) and the algorithm proposed in [26,44] are given in tables 2 and 3. We expect (see appendix A.3) an  $O(\tau_c)$  error for the algorithm proposed in [26,44] and an  $O(\tau_c^2)$  error for the algorithm presented in this paper, where  $-\Delta \tau/(2n_t) < \tau_c < \Delta \tau/(2n_t)$ . Fitting the results to the form  $a_0(n_t)^{a_1}$  gave the results presented in table 4.

First, consider the results for the algorithm presented in [26,44]. Comparing the raw data with  $\Delta \tau$  and  $\Delta \tau^2$  in tables 2 and 3 suggests that the energy conservation is dominated by  $O(\Delta \tau)$  terms. This is also indicated by the results of the fits in table 4. Furthermore,  $\Delta E_0/\tau_c$  is large and constant (there are still some large contributions from the standard leapfrog part of our algorithm at  $n_t = 1$ ), suggesting that the violation in energy conservation is dominated

			[26]			section 4.1			
$n_t$	$1/n_t$	$1/n_t^2$	$ \Delta E_0 $	$\frac{\Delta E_0}{\Delta E_0(n_t=1)}$	$\Delta \tau \frac{\Delta E_0}{\tau_c}$	$ \Delta E $	$\frac{\Delta E}{\Delta E(n_t=1)}$	$\Delta \tau \frac{\Delta E}{\tau_c}$	
1	1.000	1.000	0.296(30)	1.000(101)	1.35(12)	0.105(23)	1.000(215)	0.94(23)	
2	0.500	0.250	0.133(13)	0.451(44)	1.16(10)	0.0114(30)	0.109(28)	0.16(3)	
3	0.333	0.111	0.099(11)	0.335(37)	1.12(9)	0.0030(5)	0.028(4)	0.08(2)	
4	0.250	0.063	0.064(7)	0.217(25)	1.16(10)	0.0027(16)	0.026(2)	0.08(2)	
5	0.200	0.040	0.059(6)	0.198(19)	1.16(9)	0.0011(4)	0.011(4)	0.07(3)	
6	0.167	0.028	0.045(5)	0.151(16)	1.12(9)	0.00049(9)	0.005(1)	0.03(1)	
7	0.143	0.020	0.036(4)	0.123(14)	1.12(9)	0.00037(8)	0.004(1)	0.06(2)	

Table 3

The energy difference  $\Delta E$  for the reflection correction algorithm 2 compared with the molecular dynamics time step,  $\Delta \tau = 1/(30n_t)$ . For comparison, results for the algorithm given in [26],  $\Delta E_0$ , are also included.

	$a_0$	$a_1$	$\chi^2$
$\Delta E_0 \ (\ [26])$	$0.119(^{+0.027}_{-0.026})$	$-1.271(^{+0.183}_{-0.173})$	0.52
$\Delta E$ (section 4.1)	$0.058(^{+0.009}_{-0.009})$	$-2.642(^{+0.137}_{-0.139})$	1.11
$\Delta E_0$ [26])	$0.291(^{+0.037}_{-0.036})$	$-1.044(^{+0.094}_{-0.092})$	0.92
$\Delta E$ (section 4.1)	$0.083(^{+0.029}_{-0.026})$	$-2.879(^{+0.266}_{-0.245})$	4.01

Table 4

Fits and  $\chi^2$  values for the data presented in tables 2 and 3 for the functional form  $\Delta E = a_0(n_t)^{a_1}$  for transmission (top) and reflection (bottom). The errors are the 68% confidence levels for the fit.

by a large  $O(\tau_c)$  term. For the energy differences given by our algorithm, a different picture emerges: the violation in energy conservation is dominated by the  $O(\Delta \tau^3)$  terms from the normal leapfrog part (steps 1,2,6 and 7) of the algorithm, while the  $O(\tau_c^2)$  error which we expect from the correction steps (steps 3-5 in algorithm 2) is small. This encouraging picture has to be confirmed on larger lattices and smaller masses.

#### 5.2 Polyakov loop and Plaquette

Next we calculate several observables to check that we get sensible numbers (although on our small lattices and large masses there is little point in trying to extract any physical values). Here we look at the value of the plaquette — or, equivalently, the average gauge energy per lattice site,  $S_g = \left\langle 1 - \frac{1}{2N_C} (U_{\mu\nu} + U^{\dagger}_{\mu\nu}) \right\rangle$ ) — and the real part of the Polyakov loop.

The values of the gauge energy per lattice site and the Polyakov loop for one of our ensembles are plotted against computer time in figure 5 (other ensembles are similar). Both the plaquette and the Polyakov loop are stable over

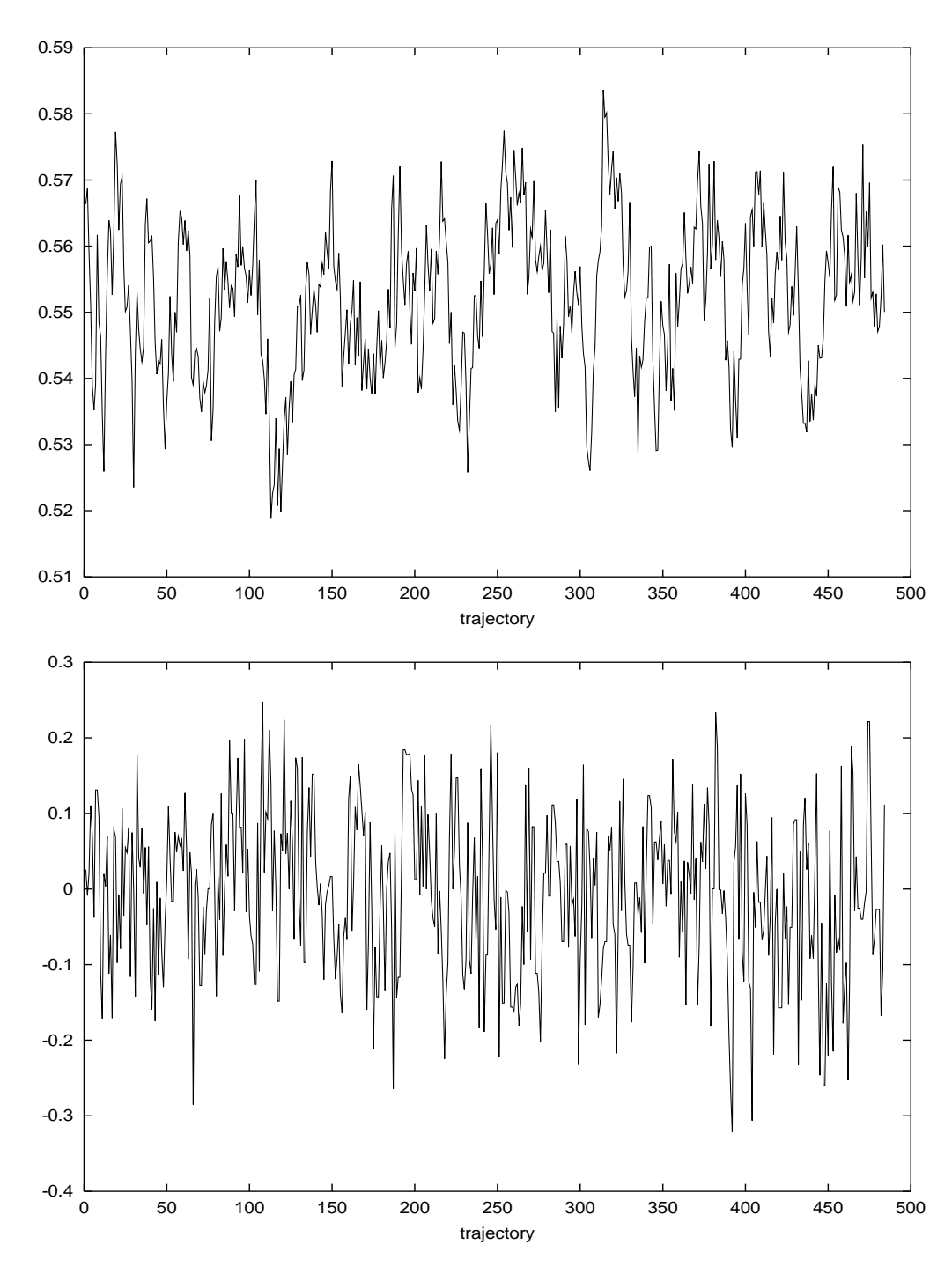


Fig. 5. The gauge energy per lattice site (top) and Polyakov loop (bottom) for each trajectory on the  $4^4$ ,  $\mu=0.5$ ,  $\kappa=0.225$  ensemble.

computer time. The average Polyakov loop, given in tables 5 and 6 is small for all our configurations, suggesting that the configurations are all confined. The average value of  $S_g$  per lattice site is given in tables 5 and 6. The statistical errors on  $S_g$  shown in these tables were obtained by calculating the jackknife error  $\sigma_j^{(n_j)}$  with  $n_j$  consecutive configurations in each bin. The jack-

$\mu$	$\langle S_g \rangle$	$ au_j$	$P_l$	κ	$\langle S_g \rangle$	$ au_j$	$P_l$
0.05	0.5754(10)	$25.05(^{+32.57}_{-12.63})$	0.0716(40)	0.18	0.5485(14)	$6.31(^{+1.66}_{-1.30})$	0.0137(31)
0.1	0.5733(7)	$12.76(^{+4.07}_{-4.71})$	0.0778(51)	0.19	0.5522(8)	$3.77(^{+0.71}_{-0.59})$	0.0153(58)
0.2	0.5678(14)	$11.90(^{+4.36}_{-3.21})$	0.0506(61)	0.2	0.5555(10)	$6.71(^{+1.55}_{-1.21})$	0.0054(50)
0.3	0.5638(8)	$4.60(^{+3.19}_{-1.94})$	0.0376(55)	0.21	0.5573(8)	$1.82(^{+0.71}_{-0.54})$	0.0241(80)
0.4	0.5570(9)	$3.98(^{+0.74}_{-0.62})$	0.0223(65)	0.22	0.5560(11)	$1.88(^{+2.14}_{-1.88})$	0.0266(94)
0.5	0.5523(13)	$4.46(^{+0.77}_{-0.94})$	0.0050(80)	0.23	0.5528(14)	$5.26(^{+1.36}_{1.08})$	0.0015(69)

Table 5

The average gauge energy per lattice site,  $\langle S_g \rangle$ , the real part of the Polyakov loop  $P_l$  and jackknife autocorrelation lengths for the plaquette, for the  $4^4$   $\kappa = 0.225$  ensembles (left) and the  $\mu = 0.5$  ensembles (right).

$\mu$	$\langle S_g \rangle$	$ au_j$	$P_l$
0.05	0.5353(10)	$9.97(^{+1.71}_{-1.48})$	0.0082(48)
0.1	0.5350(6)	$8.59(^{+0.79}_{-0.62})$	0.0049(33)
0.3	0.5230(19)	$10.93(^{+2.73}_{-2.18})$	0.0018(28)

Table 6

The average gauge energy per lattice site,  $\langle S_g \rangle$ , the real part of the Polyakov loop  $P_l$  and jackknife autocorrelation lengths for the  $6^4$  ensembles.

knife method should give a stable value when  $n_j \gg \tau_i$ , the autocorrelation length. By fitting the jackknife errors to the curve  $\sigma_j^{(n_j)} = a + b(1 - e^{-n_j/\tau_j})$  (the errors on  $\sigma_j^{(n_j)}$  were calculated using the bootstrap method) we can get an estimate of the value of the plateau ( $\sigma_j = a + b$ ), and a measure,  $\tau_j$ , of the exponential autocorrelation length. On the  $4^4$  lattices, the autocorrelation length is small at the larger masses, but increases roughly as  $1/\mu$  as we decrease the mass. On the larger lattices, the autocorrelation time is more stable with the mass. We were not able to obtain a reliable estimate of the integrated auto-correlation time on these small lattices.

#### 5.3 Topological susceptibility

The average values of the topological charge,  $Q_f = n_- - n_+$  ( $n_{\pm}$  is the number of positive/negative chirality zero modes), and of  $Q_f^2$  are given in tables 7 and 8 and are plotted in figure 6. The tables show that the average values of  $Q_f$  are generally close to 0, suggesting that we are correctly sampling the topological sectors.

The topological susceptibility, which is proportional to  $\langle Q_f^2 \rangle$ , can be related to the quark mass using chiral perturbation theory [63,64,65]. It is expected that at low quark masses the topological susceptibility should be proportional

$\mu$	$m_b$	$< Q_f^2 >$	$< Q_f >$	$n_{\rm conf}$	$\kappa$	$< Q_f^2 >$	$< Q_f >$	$n_{\rm conf}$
0.05	0.19	0.019(6)	-0.011(5)	734	0.18	0.000(0)	0.000(0)	459
0.1	0.40	0.118(18)	0.021(33)	959	0.19	0.003(4)	0.004(4)	733
0.2	0.89	0.343(36)	0.044(34)	868	0.2	0.044(16)	-0.001(14)	760
0.3	1.52	0.421(41)	-0.085(35)	967	0.21	0.255(35)	0.014(41)	442
0.4	2.37	0.507(46)	0.034(39)	905	0.22	0.461(44)	-0.047(62)	706
0.5	3.56	0.480(62)	0.057(47)	523	0.23	0.667(89)	0.088(66)	433

Table 7

The average values of the topological charge  $Q_f$ ,  $Q_f^2$ , and the number of configurations, for the  $4^4 \kappa = 0.225$  ensembles(left) and the  $4^4 \mu = 0.5$  ensembles (right).  $m_b$  is the bare fermion mass, given by equation (10).

$\mu$	$m_b$	$< Q_f^2 >$	$< Q_f >$	$n_{\rm conf}$
0.05	0.19	0.063(21)	-0.008(21)	377
0.1	0.40	0.138(22)	0.026(20)	350
0.3	1.52	0.493(62)	0.086(61)	420

Table 8

The average values of the topological charge  $Q_f$ ,  $Q_f^2$ , and the number of configurations, for the  $6^4$  ensembles.  $m_b$  is the bare fermion mass.

to the quark mass, the square of the pion mass:

$$\chi = \langle Q_f^2 \rangle V \sim \frac{f_\pi^2 m_\pi^2}{2N_E} + O(m_\pi^4).$$
(48)

There have been several attempts to verify this relation in recent years (for recent examples, see [66,67]), with mixed results. At larger quark masses, the topological susceptibility should tend asymptotically towards its quenched value. The transition between the two forms, in a large volume, is expected to be around 50-90 MeV [68]. Our bare quark masses, which we estimate (based on our early calculations of the lattice spacing on our 6<sup>4</sup> ensembles) range from about 100 MeV to a few GeV, should be in the transitional region between the two known limits: we can not expect to see a linear decrease with the quark mass. However, we do see a clear decrease in the topological susceptibility, and our results are not inconsistent with the expected functional form, although again we emphasise that our lattices are far too small to draw any meaningful conclusions.

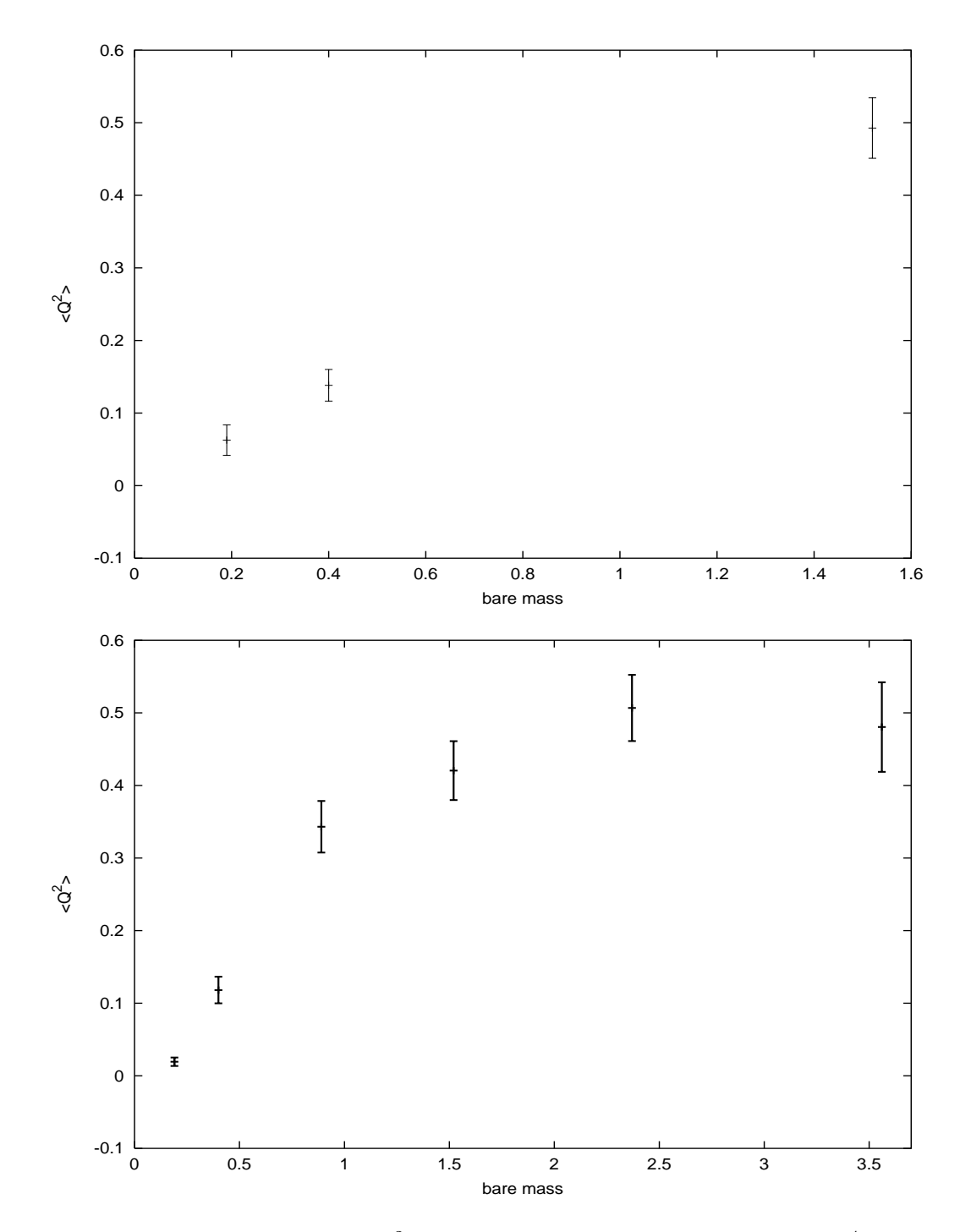


Fig. 6. The ensemble average of  $Q_f^2$  plotted against bare quark mass on the  $6^4$  (top) and  $4^4$  (bottom) ensembles.

## 5.4 Tuning $d_{max}$ .

As we remarked earlier, it is important to tune the parameter  $d_{\text{max}}$ . A high  $d_{\text{max}}$  would lead to many topological charge changes, and therefore a short

condition	$n_{ m conf}$	AR	$n_{\mathrm{top}}$	$< Q_f^2 >$	$\langle S_g \rangle$	< P <sub>l</sub> >
d  > 0.5	904	85%	0.944(50)	0.384(39)	0.5634(12)	0.0415(44)
d  > 0.45	913	86%	0.860(53)	0.398(45)	0.5623(7)	0.0324(54)
d  > 0.4	691	87%	0.847(49)	0.419(35)	0.5646(12)	0.0408(66)
d  > 0.35	933	88%	0.704(53)	0.439(25)	0.5635(10)	0.0367(56)
d  > 0.3	938	90%	0.629(45)	0.383(37)	0.4649(8)	0.0302(72)
d  > 0.25	967	90%	0.567(49)	0.421(41)	0.5638(8)	0.0376(55)
d  > 0.2	927	92%	0.481(40)	0.443(42)	0.5643(12)	0.0342(67)
d  > 0.15	873	88%	0.373(40)	0.394(31)	0.5632(10)	0.0301(50)
$1 + \frac{d_2}{\sum_k (\eta_k^2, \Pi)^2} > 0$	591	91%	1.012(75)	0.376(47)	0.5646(20)	0.0326(69)

Table 9

The acceptance rate, number of topological charge changes per trajectory  $n_{\rm top}$ , and average values of  $Q_f^2$ ,  $S_g$  and  $P_l$  for  $4^4$  ensembles generated at  $\mu=0.3$ ,  $\kappa=0.225$  and  $\beta=5.4$ , but with different reflection conditions.

topological autocorrelation length, but would lead to a low acceptance rate, because it would frequently lead to  $s_1^1 = -1$  in equations (44) and (47). A low  $d_{\text{max}}$  would have a higher acceptance rate, but fewer topological charge changes. The optimum value of  $d_{\text{max}}$ , would therefore be the largest value before the acceptance rate dropped to low levels. In this study, we set  $d_{\text{max}} = 0.25$ , since we observed that  $1 \lesssim (\eta, \Pi)^2 \lesssim 2$ , and this would very infrequently lead to  $s_1^1 = -1$ .

In table 9, we show how varying  $d_{\rm max}$  affects the acceptance rate, and the number of topological charge changes per trajectory increases with  $d_{\rm max}$ , while the acceptance rate is stable up to  $d_{\rm max}=0.5$ . This is because although the condition  $s_2=-1$  is frequently satisfied at larger  $d_{\rm max}$ , the violation in energy conservation ( $\sim -4d$ ) is not large enough to seriously affect the acceptance rate. The number of topological charge changes per trajectory with  $d_{\rm max}=0.5$  is similar to that given by the momentum dependent reflection condition  $1+d_2/\sum_k(\eta_k^2,\Pi_-)^2>0$ , which will always conserve energy but might have a small violation in area conservation, with only a 6% smaller acceptance rate, although this might change with different lattice parameters. Table 9 also confirms that the ensemble averages of the topological susceptibility, plaquette, and Polyakov loop are independent of  $d_{\rm max}$ .

#### 5.5 Computer performance.

The timings to generate a  $4^4$  trajectory are shown in table 10. These timings are based on running on 4 nodes of the cluster computer ALiCE. The  $6^4$  ensembles (table 11) were generated on 8 nodes, and the  $8^4$  ensembles on

$\mu$	Time	$n_{md}$	AR	$\kappa$	Time	$n_{md}$	AR
0.05	2322(130)	50	94%	0.18	1150(40)	30	92%
0.1	1713(200)	30	87%	0.19	1339(80)	30	95%
0.2	1782(130)	30	87%	0.2	1275(70)	30	92%
0.3	1779(110)	30	90%	0.21	2192(100)	30	91%
0.4	1836(180)	30	87%	0.22	2485(130)	30	90%
0.5	1972(220)	30	90%	0.23	1937(190)	30	90%

Table 10

The average timings for one trajectory (in seconds), the number of molecular dynamics steps and the acceptance rate for the  $\kappa = 0.225$  ensembles (left), and the  $\mu = 0.5$  ensembles (right). The total time of the trajectory,  $\Delta \tau n_{md}$ , is equal to 1.

16 nodes. We used CG with relaxation and preconditioning [48] to perform the inversion, which has an approximately factor of 4 gain over straight CG. Our timings are, perhaps surprisingly, (roughly) independent of the mass, although we expect this to change on larger and less well conditioned matrices. However, the scaling of the computer time with mass will be better than the  $\mu^{-3}$  behaviour which we expect for Wilson or staggered fermions because there are fewer crossings at small masses. It can be seen by comparing the timings on the  $\mu = 0.5$  ensembles (table 10) below and above the critical  $\kappa$  that at this large mass the time needed for the crossings was around 40% of the total computer time (there are usually 3-4 reflection or transmission steps per trajectory at  $\mu = 0.5$  and  $\kappa$  well above the critical  $\kappa$ ). The acceptance rate was stable (and admittedly rather high) for all our 4<sup>4</sup> ensembles. We increased the number of molecular dynamics steps  $(n_{md})$  to 50 (keeping  $\Delta \tau n_{md} = 1$ ) for the 4<sup>4</sup> ensemble generated with  $\mu = 0.05$  and  $\kappa = 0.225$ to counter the large fermionic force in non trivial topological sectors (see section 5.1), but otherwise we did not have to change the trajectory length as we changed the mass to maintain the acceptance rate. On our larger lattices, we had to increase  $n_{md}$  at lower masses. We estimate, assuming that the time for an HMC sweep will scale with the volume as  $V^{1.25}$  (our current volume scaling is around  $V^{1.5}$ . but we expect this to improve as we move to larger lattices), that we will need around 10<sup>15</sup> floating point operations for a 12<sup>4</sup> ensemble at these masses. According to this crude estimate is accurate, one would expect small simulations with dynamical overlap fermions on 12<sup>4</sup> or similar lattices to be feasable on the next generation of Teraflop computers. To run at smaller masses, or larger lattices, we shall need to either develop some further preconditioning or wait around 5-6 years for more computing power.

 $<sup>^7</sup>$  In parallel computations, we estimated by explicity calculating the number of floating point operations for one trajectory that ALiCE runs at around 0.4GFlops/node for the  $4^4$  ensembles and 0.7GFlops/node for the  $6^4$  and  $8^4$  ensembles.

Configuration	Time	$n_{md}$	AR
$6^4 \ \mu = 0.05$	6714(250)	40	84%
$6^4 \ \mu = 0.1$	6674(240)	40	86%
$6^4 \ \mu = 0.3$	5535(110)	30	79%
$8^4 \ \mu = 0.1$	30049(1087)	50	79%
$8^4 \ \mu = 0.3$	26456(540)	40	80%

Table 11

The average timings for one trajectory (in seconds), the number of molecular dynamics steps, and the acceptance rate on the larger lattices, with  $\kappa = 0.2$ . The total time of the trajectory, is equal to 1.

#### 6 Conclusions

We have constructed a Hybrid Monte Carlo algorithm for lattice QCD that is capable of gernerating gauge field configurations with two flavors of dynamical overlap fermions. The proposed HMC algorithm will allow us to explore the low quark mass regime of lattice QCD.

The main conceptual difficulty with constructing a dynamical overlap algorithm is the Dirac delta function arising in the fermionic force caused by zero-crossings of the low eigenvalues of the Wilson kernel within the overlap operator. Treating the low mode crossings within the molecular dynamics part of the HMC explicitly, the remaining energy violation is comparable to the  $O(\Delta \tau^2)$  error of the standard HMC leap-frog integration over the entire trajectory. The algorithm treats the lowest Wilson operator eigenvalues exactly, and can cope with multiple eigenvalue crossings in the same time step.

We have tested our algorithm on lattices with sizes ranging from  $4^4$  to  $8^4$ , calculating a set of basic observables. Despite large finite-size effects on lattices of these sizes, we do get results for, e.g. the topological suseptability which are qualitatively as expected.

The main practical difficulty with generating dynamical overlap configurations, namely that the calculation of the matrix sign function is very costly, remains. We were able to reduce the computational costs by a considerable factor employing novel preconditions and relaxation techniques developed in earlier papers of this series [47,48]. Work in this area is continuing.

We have generated ensembles on  $8^4$  lattices. Together with our early work on  $10^4$ ,  $12^4$  and  $10^320$  lattices, we have demonstrated that these lattice sizes are within the range of today's computers.

As computing power continues to improve, and assuming that some additional

gain from preconditioning is possible, it should be possible to start running dynamical overlap simulations on more realistic lattices and lower masses in the near future.

#### 7 Acknowledgements

We would like to thank S Katz, G. Schierholz, A. Borici and K. Szabo and in particular Z. Fodor for many important discussions and comparisons of results. NC was supported by the EU Marie-Curie fellowship Number MC-EIF-CT-2003-501467. Furthermore, this research is part of the EU integrated infrastructure initiative HADRONPHYSICS project under contract number RII3-CT-2004-506078 as well as the EU integrated infrastructure project I3HP "Computational Hadron Physics" contract No. RII3-CT-2004-506078. GA was supported by the Deutsche Forschungsgemeinschaft under grant Li 701/4-1. The numerical work was carried out on the Wuppertal cluster computer ALiCE. We thank Boris Orth and Norbert Eicker for their help with this computer.

#### A Detailed balance and the size of the correction step error.

In this appendix we shall demonstrate that the general correction update (42) satisfies detailed balance. Extending this proof to our slighty modified update in equations (44) and (47) is trivial.

#### A.1 Detailed balance: Reversibility

We know that the initial and final leapfrog steps (steps 1 and 2, and 6 and 7) in our algorithm 2 are reversible. We just have to show that the correction steps (steps 3, 4 and 5) are reversible.

Here, we shall just give the proof of reversibility for the transmission correction step in algorithm 2. The proof for the reflection update is entirely analogous.

#### A.1.1 The momentum update

We shall assume that when we reverse the sign of  $\Delta \tau$ ,  $d_k \to -d_k \ \forall k$ . This condition is satisfied on our updates, because  $\tau_c$  and  $\eta_k^j$  remain constant,  $F^+ \to F^-$ , and  $d \to -d$ , since the sign of the smallest eigenvalue is opposite on the

reverse update. Our general transmission momentum update (42) reads

$$\Pi^{+} = \Pi^{-} - \tau_{c}(F^{-} - F^{+}) + \tau_{c}\eta(\eta, F^{-} - F^{+}) + \frac{1}{3}\operatorname{Tr}(F^{-} - F^{+}) + 
\eta(\Pi^{-}, \eta) \left( \sqrt{1 + \frac{d_{1}}{(\Pi^{-}, \eta)^{2}}} - 1 \right) 
+ \sum_{k} \left( \eta_{1}^{k}(\eta_{1}^{k}, \Pi^{-} - \frac{\tau_{c}}{2}(F^{-} + F^{+})) + \eta_{1}^{k}(\eta_{2}^{k}, \Pi^{-} - \frac{\tau_{c}}{2}(F^{-} + F^{+})) \right) \times 
\left( \sqrt{1 + \frac{d_{k}}{(\eta_{1}^{k}, \Pi^{-} - \frac{\tau_{c}}{2}(F^{-} + F^{+}))^{2} + (\eta_{2}^{k}, \Pi^{-} - \frac{\tau_{c}}{2}(F^{-} + F^{+}))^{2}}} - 1 \right),$$
(A.1)

so that

$$(\Pi^{+}, \eta) = (\Pi^{-}, \eta) \sqrt{1 + \frac{d_{1}}{(\Pi^{-}, \eta)^{2}}}$$

$$(\Pi^{+} + \frac{\tau_{c}}{2}(F^{-} + F^{+}), \eta_{k_{i}}) = (\eta_{k_{i}}, \Pi^{-} - \frac{\tau_{c}}{2}(F^{-} + F^{+})) \times$$

$$\left(\sqrt{1 + \frac{d_{k}}{(\eta_{1}^{k}, \Pi^{-} - \frac{\tau_{c}}{2}(F^{-} + F^{+}))^{2} + (\eta_{2}^{k}, \Pi^{-} - \frac{\tau_{c}}{2}(F^{-} + F^{+}))^{2}} - 1\right). \tag{A.2}$$

The time-reverse update, with  $\Delta \tau \to -\Delta \tau$  is given by

$$\Pi'_{-} = \Pi^{+} + \tau_{c}(F^{+} - F^{-}) - \tau_{c}\eta(\eta, F^{+} - F^{-}) - \frac{1}{3}\operatorname{Tr}(F^{-} - F^{+}) + \\
\eta(\Pi^{+}, \eta) \left(\sqrt{1 - \frac{d_{1}}{(\Pi^{+}, \eta)^{2}}} - 1\right) + \\
\sum_{k} \left(\eta_{1}^{k}(\eta_{1}^{k}, \Pi^{+} - \frac{\tau_{c}}{2}(F^{-} + F^{+})) + \eta_{2}^{k}(\eta_{2}^{k}, \Pi^{+} - \frac{\tau_{c}}{2}(F^{-} + F^{+}))\right) \times \\
\left(\sqrt{1 - \frac{d_{k}}{(\eta_{1}^{k}, \Pi^{+} - \frac{\tau_{c}}{2}(F^{-} + F^{+}))^{2} + (\eta_{2}^{k}, \Pi^{+} - \frac{\tau_{c}}{2}(F^{-} + F^{+}))^{2}}} - 1\right). \tag{A.3}$$

We note that

$$(\Pi^{+}, \eta) \left( \sqrt{1 - \frac{d_{1}}{(\Pi^{+}, \eta)^{2}}} - 1 \right)$$

$$= (\Pi^{-}, \eta) \sqrt{1 + \frac{d_{1}}{(\Pi^{-}, \eta)^{2}}} \left( \sqrt{1 - \frac{d_{1}}{(\Pi^{-}, \eta)^{2}} \left( 1 + \frac{d_{1}}{(\Pi^{-}, \eta)^{2}} \right)} - 1 \right)$$

$$= (\Pi^{-}, \eta) \left( 1 - \sqrt{1 + \frac{d_{1}}{(\Pi^{-}, \eta)^{2}}} \right)$$

$$(A.4)$$

$$(\Pi^{+} - \frac{\tau_{c}}{2} (F^{-} + F^{+}), \eta_{1}^{k}) \times$$

$$\left( \sqrt{1 - \frac{d_{k}}{(\eta_{1}^{k}, \Pi^{+} + \frac{\tau_{c}}{2} (F^{-} + F^{+}))^{2}} + (\eta_{2}^{k}, \Pi^{+} - \frac{\tau_{c}}{2} (F^{-} + F^{+}))^{2}} - 1 \right)$$

$$= - (\Pi^{-} - \frac{\tau_{c}}{2} (F^{-} + F^{+}), \eta_{1}^{k}) \times$$

$$\left( \sqrt{1 + \frac{d_{k}}{(\eta_{1}^{k}, \Pi^{-} - \frac{\tau_{c}}{2} (F^{-} + F^{+}))^{2}} + (\eta_{2}^{k}, \Pi^{-} - \frac{\tau_{c}}{2} (F^{-} + F^{+}))^{2}} - 1 \right)$$

$$(A.5)$$

Combining (A.1), (A.3), (A.4) and (A.5) gives us  $\Pi'_{-} = \Pi^{-}$ , so the momentum update is reversible.

#### A.1.2 The gauge field update

The gauge field update is

$$U^{+} = e^{-i\tau_c \Pi^{+}} e^{i\tau_c \Pi^{-}} U^{-}. \tag{A.6}$$

Switching  $\Delta \tau \to -\Delta \tau$  gives

$$U'_{-} = e^{-i\tau_c \Pi^{-}} e^{i\tau_c \Pi^{+}} U^{+}, \tag{A.7}$$

which leads to  $U'_{-} = U^{-}$ , indicating that the gauge field update is reversible.

#### A.2 Detailed Balance: area conservation

#### A.2.1 Transmission

In this section, we will prove that the transmission update, given by algorithm 2 and using equation 42, is area conserving. For simplicity, we shall assume that  $d_1$  is a function of the gauge field at the crossing only and has no additional

dependence on  $\Pi$ , and all the other  $d_k$ s are functions of the gauge field of the crossing and  $(\eta, \Pi)$  only. The matrices  $\eta_j^i$ , and the fermionic forces  $F^{\pm}$  are just functions of the gauge field at the crossing. These conditions can be relaxed, but we do not need to do so for the purposes of this paper.

 $D_i$  is a derivative of the gauge fields U, defined as

$$D_{i}f(U) = \lim_{h \to 0} \frac{\partial}{\partial h} f\left(e^{ihT_{i}}U\right), \tag{A.8}$$

where  $T_i$  are some suitable generators of the SU(N) gauge group (e.g. in SU(3),  $T_i = \lambda_i/2$ , where  $\lambda_i$  are the Gell-Mann matrices). We can write the gauge fields in terms of  $N^2 - 1$  parameters  $r_i$  so that

$$D_i f(U) = \frac{\partial}{\partial r_i} f(U). \tag{A.9}$$

Similarly, we can define coordinates for the momentum  $\Pi$  and the matrix  $\eta$  in terms of the generators T:

$$\Pi_{\mu}(x) = \pi_i^{x\mu} T_i, \qquad \eta_{\mu}(x) = \eta_i^{x\mu} T_i, \qquad F_{\pm} - \frac{1}{3} \text{Tr}(F_{\pm}) = f_{\pm i}^{x\mu} T_i, 
\eta_{j,\mu}^k(x) = n_{j,i}^{k,x\mu} T_i. \tag{A.10}$$

x refers to the lattice site, and  $\mu$  is a direction index. The normalisation condition  $(\eta, \eta) = 1$  implies that  $n_j^k$  is normalised according to  $n_{j,i}^{k,x\mu} n_{j,i}^{k,x\mu} = 2$ . For notational convenience, we shall define

$$\begin{split} N_{i}^{x\mu}(U,\Pi) = & \frac{1}{2} \eta_{i}^{x\mu}(U) \eta_{j}^{y\nu}(U) \pi_{j}^{y\nu} \left( \sqrt{1 + \frac{4d_{1}}{(\eta_{k}^{z\rho}(U)\pi_{k}^{z\rho})^{2}}} - 1 \right) - \\ & \tau_{c} \left( \delta_{ij} \delta^{xy} \delta^{\mu\nu} - \eta_{i}^{x\mu}(U) \eta_{j}^{y\nu}(U) \right) \left( f_{-j}^{y\nu}(U) - f_{+j}^{y\nu}(U) \right) + \\ & \sum_{k} \left( n_{1,i}^{k,x\mu}(U) N_{e1}^{k}(U,\Pi) + n_{2,i}^{k,x\mu}(U) N_{e2}^{k}(U,\Pi) \right) \\ & \left( \sqrt{1 + \frac{d_{k}}{(N_{e1}^{k}(U,\Pi))^{2} + (N_{e2}^{k}(U,\Pi))^{2}}} - 1 \right). \end{split} \tag{A.11}$$
 
$$N_{e1}^{k} = \frac{1}{2} \left( n_{1,j}^{k,z\rho} \left( \pi_{j}^{z\rho} - \frac{\tau_{c}}{2} (f_{+j}^{z\rho} - f_{-j}^{z\rho}) \right) \right), \tag{A.12}$$

The generator of a time update  $\Delta \tau$  is

$$e^{\Delta \tau \frac{\partial}{\partial \tau}} = e^{\Delta \tau \left(\frac{\partial \pi_i}{\partial \tau} \frac{\partial}{\partial \pi_i} + \frac{\partial r_i}{\partial \tau} \frac{\partial}{\partial r_i}\right)}$$

$$= e^{\Delta \tau \left(-\frac{\partial E}{\partial r_i} \frac{\partial}{\partial \pi_i} + \frac{\partial E}{\partial \pi_i} \frac{\partial}{\partial r_i}\right)}$$

$$= e^{\Delta \tau \hat{H}}. \tag{A.13}$$

For the standard leapfrog update, we define the operators

$$\hat{P} = e^{\frac{\Delta\tau}{2}F_i'\frac{\partial}{\partial\pi_i}}$$

$$\hat{Q} = e^{\frac{\Delta\tau}{2}\pi_i\frac{\partial}{\partial r_i}},$$
(A.14)

then we have

$$\hat{P}f(\pi,r) = f(\pi + F'\frac{\Delta\tau}{2}, r) \qquad \hat{Q}f(\pi,r) = f(\pi, r + \frac{\Delta\tau}{2}\pi). \tag{A.15}$$

F' is the total force in the momentum update (the sum of the gauge field and fermionic forces). The standard leapfrog update is given by

$$\hat{P}\hat{Q}\hat{Q}\hat{P} = e^{\Delta\tau(\hat{H} + O(\Delta\tau^2))}.$$
(A.16)

 $\hat{P}\hat{Q}\hat{Q}\hat{P}$  is manifestly area conserving, because the operators  $\hat{P}$  and  $\hat{Q}$  are area conserving.

For the correction step, we need to define two new update operators,  $\hat{P}_c$  and  $\hat{Q}_c$ , so that  $\hat{Q}_c f(\pi, r) = f(\pi, r - \tau_c \pi)$  and  $\hat{P}_c f(\pi, r) = f(\pi + N_i, r)$ .  $\hat{P}_c$  and  $\hat{Q}_c$  are

$$\hat{P}_c = 1 + N_i \frac{\partial}{\partial \pi_i} + \frac{1}{2} N_i N_j \frac{\partial^2}{\partial \pi_i \pi_j} + \frac{1}{6} N_i N_j N_k \frac{\partial^3}{\partial \pi_i \pi_j \pi_k} + \dots$$

$$\hat{Q}_c = 1 - \tau_c \pi_i \frac{\partial}{\partial r_i} + \frac{1}{2} \tau_c^2 \pi_i \pi_j \frac{\partial^2}{\partial r_i r_j} + \frac{1}{6} \tau_c^3 \pi_i \pi_j \pi_k \frac{\partial^3}{\partial r_i r_j r_k} + \dots$$
(A.17)

Because  $[\partial/\partial r_i, \tau_c] \neq 0$  and  $[\partial/\partial r_i, N_j] \neq 0$ , we cannot factorise  $\hat{P}_c$  and  $\hat{Q}_c$  into a simple exponential form, although using equation (A.9) we can write

$$\hat{Q}_c U = e^{-i\tau_c \pi_i T_i} U = e^{-i\tau_c \Pi^-} U. \tag{A.18}$$

These operators by themselves are not area conserving. The full correction update is  $\hat{Q}_c^{\dagger}\hat{P}_c\hat{Q}_c$ :

$$\hat{Q}_{c}^{\dagger}\hat{P}_{c}\hat{Q}_{c}\Pi^{-} = \Pi^{-} + \frac{1}{2}\eta(\eta_{j}^{x\mu}\pi_{j}^{x\mu})\left(\sqrt{1 + \frac{4d_{1}}{(\eta_{m}^{y\nu}(\tau_{c})\pi_{m}^{y\nu})^{2}}} - 1\right) + (F^{+} - F^{-}) - \frac{1}{2}\eta\eta_{j}^{x\mu}(f_{+} - f_{-})_{j}^{x\mu} + \sum_{k}(\eta_{1}^{k}N_{e1}^{k} + \eta_{2}^{k}N_{e2}^{k})\left(\sqrt{1 + \frac{d_{k}}{(N_{e1}^{k})^{2} + (N_{e2}^{k})^{2}}} - 1\right) = \Pi^{+} \hat{Q}_{c}^{\dagger}\hat{P}_{c}\hat{Q}_{c}U^{-} = \hat{Q}_{c}^{\dagger}\hat{P}_{c}e^{-i\tau_{c}\Pi^{-}}U^{-} = \hat{Q}_{c}^{\dagger}e^{-i\tau_{c}(\Pi^{-} + N(U^{-}, \Pi^{-}))}U^{-} = e^{-i\tau_{c}(\Pi_{-} + N(U_{c}, \Pi_{-}))}e^{i\tau_{c}\Pi^{-}}U^{-} = U^{+}, \tag{A.19}$$

where d, f,  $\eta$  etc. are all calculated at the crossing gauge field  $U_c$ . Therefore, the update in algorithm 2 can be written as  $\hat{P}\hat{Q}\hat{Q}_c^{\dagger}\hat{P}_c\hat{Q}_cQP$ . We know that  $\hat{P}$  and  $\hat{Q}$  are area conserving, so we just need to show that  $\hat{Q}_c^{\dagger}\hat{P}_c\hat{Q}_c$  is also area conserving. We write the updated gauge field and momentum as q and p respectively (recalling that the initial fields were r and  $\pi$  in our notation). This gives us

$$p_{i}^{x\mu} = \hat{Q}_{c}^{\dagger} \hat{P}_{c} \hat{Q}_{c} \pi_{i}^{x\mu} = \pi_{i}^{x\mu} + \frac{1}{2} \eta_{i}^{x\mu} \pi_{j}^{y\nu} \eta_{j}^{y\nu} \left( \sqrt{1 + \frac{4d_{1}}{(\pi_{m}^{z\rho} \eta_{m}^{z\rho})^{2}}} - 1 \right) - \tau_{c} \left( \delta_{ij} \delta^{xy} \delta^{\mu\nu} - \frac{1}{2} \eta_{i}^{x\mu} \eta_{j}^{y\nu} \right) \left( f_{-j}^{y\nu} - f_{+j}^{y\nu} \right) + \sum_{k} \left( n_{1,i}^{k,x\mu} N_{e1}^{k} + n_{2,i}^{k,x\mu} N_{e2}^{k} \right) \left( \sqrt{1 + \frac{d_{k}}{(N_{e1}^{k})^{2} + (N_{e2}^{k})^{2}}} - 1 \right)$$

$$q_{i}^{x\mu} = \hat{Q}_{c}^{\dagger} \hat{P}_{c} \hat{Q}_{c} r = r_{i}^{x\mu} + \tau_{c} (\pi_{i}^{x\mu} - p_{i}^{x\mu}).$$
(A.20)

We need to show that the determinant

$$J = \begin{vmatrix} \frac{\partial p_i}{\partial \pi_m} & \frac{\partial q_i}{\partial \pi_m} \\ \frac{\partial p_i}{\partial r_m} & \frac{\partial q_i}{\partial r_m} \end{vmatrix} = 1. \tag{A.22}$$

 $r_c$  is the gauge field at the eigenvalue crossing:

$$r_{ci}^{x\mu} = \hat{Q}_c r_i^{x\mu} = r_i^{x\mu} + \pi_i^{x\mu} \tau_c. \tag{A.23}$$

Thus, we can write

$$\tau_c = \frac{(r_c^{y\nu} - r^{y\nu})_i \eta_i^{y\nu}}{\pi_j^{z\rho} \eta_j^{z\rho}},\tag{A.24}$$

$$\frac{\partial \tau_c}{\partial \pi_k^{x\mu}} = \frac{1}{\pi_i^{z\rho} \eta_i^{z\rho}} \left( \frac{\partial r_{ci}^{y\nu}}{\partial \pi_k^{x\mu}} \eta_i^{y\nu} - \tau_c \eta_k^{x\mu} + \frac{\partial \eta_j^{y\nu}}{\pi_k^{x\mu}} (r_c^{y\nu} - r^{y\nu} - \tau_c \pi^{y\nu})_j \right), \quad (A.25)$$

$$\frac{\partial \tau_c}{\partial r_k^{x\mu}} = \frac{1}{\pi_j^{z\rho} \eta_j^{z\rho}} \left( \frac{\partial r_{ci}^{y\nu}}{\partial r_k^{x\mu}} \eta_i^{y\nu} - \eta_k^{x\mu} + \frac{\partial \eta_j^{y\nu}}{\partial r_k^{x\mu}} (r_c^{y\nu} - r^{y\nu} - \tau_c \pi^{y\nu})_j \right). \tag{A.26}$$

We choose  $\eta$  so that

$$\frac{\partial r_{ci}^{y\nu}}{\partial r_{\nu}^{x\mu}} \eta_i^{y\nu} = \frac{\partial r_{ci}^{y\nu}}{\partial \pi_{\nu}^{x\mu}} \eta_i^{y\nu} = 0. \tag{A.27}$$

Hence

$$\frac{\partial \tau_c}{\partial \pi_k^{x\mu}} = \tau_c \frac{\partial \tau_c}{\partial r_k^{x\mu}} = -\tau_c \frac{\eta_k^{x\mu}}{\pi_j^{z\rho} \eta_j^{z\rho}}.$$
 (A.28)

Since  $r_c$  is a point on the surface of constant  $\lambda = 0$ , one solution to (A.27) is

that  $\eta_i$  is normal to this surface, i.e. proportional to the vector

$$\frac{\partial \lambda}{\partial r_{ci}^{x\mu}} = -\kappa \langle \psi(x) | \gamma_5 \left( (1 - \gamma_\mu) \frac{\partial U}{\partial r_{ci}^{x\mu}} \delta_{x,y+\mu} + (1 + \gamma_\mu) \frac{\partial U^{\dagger}}{\partial r_{ci}^{x\mu}} \delta_{x,y-\mu} \right) | \psi(y) \rangle. \tag{A.29}$$

We also have for any function g of  $r + \pi \tau_c$  (such as  $\eta$  or d),

$$\frac{\partial g}{\partial \pi_k^{z\rho}} = \tau_c \frac{\partial g}{\partial r_k^{z\rho}}.$$
 (A.30)

We are now in a position to write down the components of J by differentiating (A.20) and (A.21). By writing p and q as functions of  $r_c$  and  $\pi$ , we have

$$\begin{split} \left(\frac{\partial p_{i}^{x\mu}}{\partial \pi_{m}^{y\nu}}\right)_{r} &= \left(\frac{\partial p_{i}^{x\mu}}{\partial \pi_{m}^{y\nu}}\right)_{r_{c}} + \left(\frac{\partial p_{i}^{x\mu}}{\partial r_{cj}^{xp}}\right)_{\pi} \left(\frac{\partial r_{cj}^{z\rho}}{\partial \pi_{m}^{y\nu}}\right)_{r} \\ &= \left(\frac{\partial p_{i}^{x\mu}}{\partial \pi_{m}^{y\nu}}\right)_{r_{c}} + \tau_{c} \left(\frac{\partial p_{i}^{x\mu}}{\partial r_{m}^{y\nu}}\right)_{\pi} \\ &= \delta_{im}\delta_{xy}\delta_{\mu\nu} + \frac{1}{2}\eta_{i}^{x\mu}\eta_{m}^{y\nu} \left(\frac{1}{\sqrt{1 + \frac{4d_{1}}{(\pi_{n}^{c}p_{\eta_{n}^{c}p})^{2}}}} - 1\right) + \tau_{c}\frac{\partial p_{i}^{x\mu}}{\partial r_{m}^{y\nu}} + \\ &\frac{1}{2}\sum_{k}n_{1,i}^{k,x\mu}n_{1,m}^{k,y\nu} \left(-1 + \frac{1 + (N_{e2}^{k})^{2}\frac{d_{k}}{((N_{e1}^{k})^{2} + (N_{e2}^{k})^{2})^{2}}}{\sqrt{1 + \frac{d_{k}}{(N_{e1}^{k})^{2} + (N_{e2}^{k})^{2}}}}\right) + \\ &\frac{1}{2}\sum_{k}n_{2,i}^{k,x\mu}n_{2,m}^{k,y\nu} \left(-1 + \frac{1 + (N_{e1}^{k})^{2}\frac{d_{k}}{((N_{e1}^{k})^{2} + (N_{e2}^{k})^{2})^{2}}}{\sqrt{1 + \frac{d_{k}}{(N_{e1}^{k})^{2} + (N_{e2}^{k})^{2}}}}\right) - \\ &\frac{1}{2}\sum_{k}\left(n_{1,i}^{k,x\mu}n_{2,m}^{k,y\nu} + n_{2,i}^{k,x\mu}n_{1,m}^{k,y\nu}\right) \left(\frac{N_{e1}^{k}N_{e2}^{k}\frac{d_{k}}{((N_{e1}^{k})^{2} + (N_{e2}^{k})^{2})^{2}}}{\sqrt{1 + \frac{d_{k}}{(N_{e1}^{k})^{2} + (N_{e2}^{k})^{2}}}}\right) + \\ &\frac{1}{2}\sum_{k}\left(n_{1,i}^{k,x\mu}N_{e1}^{k} + n_{2,i}^{k,x\mu}N_{e2}^{k}\right)\eta_{m}^{k,y\nu}\frac{\left(\frac{\partial d_{k}}{\partial (\eta_{n}^{xp}\pi_{n}^{xp})}\right)_{r_{c}}}{\sqrt{1 + \frac{d_{k}}{(N_{e1}^{k})^{2} + (N_{e2}^{k})^{2}}}}\right) + \\ &\frac{\partial q_{i}^{x\mu}}{\partial \pi_{m}^{y\nu}} = -\tau_{e}\frac{\partial p_{i}^{x\mu}}{\partial \pi_{m}^{y\nu}} + \tau_{e}\left(\frac{\partial q_{i}^{x\mu}}{\partial r_{m}^{y\nu}} + \tau_{e}\frac{\partial p_{i}^{x\mu}}{\partial r_{m}^{y\nu}}\right). \\ &\frac{\partial q_{i}^{x\mu}}{\partial r_{m}^{y\nu}} = \delta_{im}\delta_{xy}\delta_{\mu\nu} - \frac{\eta_{m}^{y\nu}}{\eta_{i}^{z\rho}\pi^{z\rho_{i}}}(\pi_{i}^{x\mu} - p_{i}^{x\mu}) - \tau_{e}\frac{\partial p_{i}^{x\mu}}{\partial r_{m}^{y\nu}}. \end{aligned} \tag{A.32}$$

Therefore, the Jacobian is

$$J = \begin{vmatrix} \frac{\partial p_i}{\partial \pi_k} & \frac{\partial q_i}{\partial \pi_k} \\ \frac{\partial p_i}{\partial r_k} & \frac{\partial q_i}{\partial r_k} \end{vmatrix} = \begin{vmatrix} \frac{\partial p_i}{\partial \pi_i} & \frac{\partial q_i}{\partial \pi_k} + \tau_c \frac{\partial p_i}{\partial \pi_k} \\ \frac{\partial p_i}{\partial r_k} & \frac{\partial q_i}{\partial r_k} + \tau_c \frac{\partial p_i}{\partial r_k} \end{vmatrix}$$

$$= \begin{vmatrix} \frac{\partial p_i}{\partial \pi_k} - \tau_c \frac{\partial p_i}{\partial r_k} & \frac{\partial q_i}{\partial \pi_k} + \tau_c \frac{\partial p_i}{\partial \pi_k} - \tau_c \left( \frac{\partial q_i}{\partial r_k} + \tau_c \frac{\partial p_i}{\partial r_k} \right) = 0 \\ \frac{\partial p_i}{\partial r_k} & \frac{\partial q_i}{\partial r_k} + \tau_c \frac{\partial p_i}{\partial r_k} \end{vmatrix}. \tag{A.34}$$

So J is the product of the two determinants

$$\left| \frac{\partial p_i}{\partial \pi_m} - \tau_c \frac{\partial p_i}{\partial r_m} \right| = \frac{1}{\sqrt{1 + \frac{4d_1}{(\pi_z^{n\rho} \eta_z^{n\rho})^2}}}$$
(A.35)

and

$$\left| \frac{\partial q_i}{\partial r_m} + \tau_c \frac{\partial p_i}{\partial r_m} \right| = \sqrt{1 + \frac{4d_1}{(\pi_n^{z\rho} \eta_n^{z\rho})^2}}$$
 (A.36)

The two determinants (equations A.35 and A.36) can easily be calculated by using the relations  $|\delta_{ij} + N_i^a M_{ab} N_j^b| = |\delta_{ab} + M_{ab}|$  (where  $N_i^a N_i^b = \delta_{ab}$  and  $N_i^a$  are real) and  $|\delta_{ij} + v_i u_j| = 1 + v_i u_i$ , and by recalling that  $\eta_i^{x\mu}$  and  $\eta_{1,i}^{k,x\mu}$  are normalised to 2. Note that equation (A.36) would not hold if we included terms in the fermionic force parallel to  $\eta$ . Multiplying the two determinants together gives J = 1. Therefore, this procedure is area conserving.

## A.2.2 Reflection

The proof that the reflection algorithm is area conserving follows the same method as that for transmission: instead of equations (A.35) and (A.36), we get

$$\left| \frac{\partial p_i}{\partial \pi_m} - \tau_c \frac{\partial p_i}{\partial r_m} \right| = -1 \tag{A.37}$$

$$\left| \frac{\partial q_i}{\partial r_m} + \tau_c \frac{\partial p_i}{\partial r_m} \right| = -1, \tag{A.38}$$

which gives J=1.

#### A.2.3 The combined update step

There is one further requirement for area conservation to be satisfied. It is not enough for the normal update and the corrected update to be area conserving seperately; the combination of them which we use in our molecular dynamics procedure must also conserve energy. If we define  $F_T^{\Pi,U}$  as the momentum updates for reflection and transmission respectively, then, if we transmit for  $x(\Pi^-, U_C) > 0$ , and reflect for x < 0, then

$$p_i = F_{T_i}^{\Pi} \theta(x) + (1 - \theta(x)) F_{R_i}^{\Pi}$$
 (A.39)

$$q_i = \tau_c(p_i - \pi_i). \tag{A.40}$$

 $\theta(x)$  is the step function, i.e.  $\theta=1$  for x>0 and  $\theta(x)=0$  for x<0. There will be a  $\delta$ -function in the Jacobian from the differential of the step function unless

$$\left| \left( F_{Ti}^{\Pi} - F_{Ri}^{\Pi} \right) \left( \frac{\partial x}{\partial \pi_m} \right)_{U_C} \right| = 0. \tag{A.41}$$

For example, using  $d_1=4d$  and  $x=1+4d/(\eta,\Pi^-)^2$  leads to a Jacobian

$$J = 1 + (1 - x)^{2} \frac{d}{dx} \left( \frac{2\theta(x) - (1 + \sqrt{x})\theta^{2}(x)}{\sqrt{x} - 1} \right) = 1 - \delta(x).$$
 (A.42)

We need the updating procedure to satisfy

$$W_c[U] = \int d[U']P[U \leftarrow U']W_c[U'], \qquad (A.43)$$

where the probability of moving from a gauge U to the gauge field U' is  $P[U' \leftarrow U]$  and  $W_c$  is the canonical distribution for the gauge fields. This is satisfied by the detailed balance condition

$$P[U' \leftarrow U]W_c[U] = P[U \leftarrow U']W_c[U']. \tag{A.44}$$

To prove the detailed balance condition for the HMC [69], we define

$$P_{\Pi}[\Pi] = e^{-\frac{1}{2}\Pi^{2}}$$

$$P_{\Phi}[\Phi, U] = e^{-\Phi^{\dagger} \frac{1}{H^{2}[U]} \Phi}$$

$$P_{A}([\Pi', \Phi, U'] \leftarrow [\Pi, \Phi, U]) = \min \left(1, e^{-E[\Pi', \Phi, U'] + E[\Pi, \Phi, U]}\right)$$

$$P_{\Pi}P_{\Phi}W_{c}[U] = e^{-E([\Pi, \Phi, U])}$$

$$P_{MD}([\Pi', \Phi, U'] \leftarrow [\Pi, \Phi, U]) = \delta([\Pi', \Phi, U'] - T_{MD}[\Pi, \Phi, U]), \qquad (A.45)$$

where  $T_{MD}$  is the molecular dynamics trajectory, and

$$P[U' \leftarrow U] = \int d[\Pi] d[\Pi'] d[\Phi] P_{\Pi}[\Pi] P_{\Phi}[\Phi, U]$$

$$P_A([\Pi', \Phi, U'] \leftarrow [\Pi, \Phi, U]) P_{MD}([\Pi', \Phi, U'] \leftarrow [\Pi, \phi, U]). \quad (A.46)$$

It can be shown that

$$P[U' \leftarrow U]W_{c}[U] - P[U \leftarrow U']W_{c}[U'] = \Delta_{\delta}(U, U')$$

$$\Delta_{\delta}(U, U') = \int d[\phi]d[\Pi]d[\Pi']\min\left(e^{-E([\Pi, \Phi, U])}, e^{-E([\Pi', \Phi, U'])}\right)$$

$$\sum_{N_{\text{crossings}}} \prod_{k=2}^{N_{\text{crossings}}} \int d[U_{c}^{1}]d[U_{c}^{k}] \left(\prod_{j=1}^{N_{\text{crossings}}} \left(1 - \delta\left(1 + \frac{4d(U_{c}^{j})}{(\eta(U_{c}^{j}), \Pi_{j}^{-})^{2}}\right)\right) - 1\right)$$

$$\delta([\Pi, \Phi, U] - T_{MD}^{0}([\Pi_{1}^{-}, \Phi, U_{c}^{1}]))\delta([\Pi_{k-1}^{+}, \Phi, U_{c}^{k-1}] - T_{MD}^{k-1}([\Pi_{k}^{-}, \Phi, U_{c}^{k}]))$$

$$\delta([\Pi_{N_{\text{crossings}}}^{+}, \Phi, U_{c}^{N_{\text{crossings}}}] - T_{MD}^{N_{\text{crossings}}}([\Pi', \Phi, U'])). \tag{A.47}$$

There are  $N_{\text{crossings}}$  eigenvalue crossings during the trajectory, each crossing at a particular gauge field  $U_c^k$ , and we have to sum over all the possible  $N_{\text{crossings}}$ . It seems unlikely that  $\Delta_{\delta}=0$ , and therefore, if the Jacobian contains a  $\delta$ -function, the detailed balance condition A.44 will not be satisfied. However, this does not mean that the canonical ensemble is not the equilibrium ensemble of the updating procedure: to satisfy (A.43) we need to show that  $\sum_{U'} \Delta_{\delta}(U', U) = 0$ . A sufficient (but not necessary) solution for this condition is  $\Delta_{\delta}(U', U) + \Delta_{\delta}(U, U') = 0 \forall U, U'$ . When  $N_{\text{crossings}} = 1$ , we have

$$\begin{split} &\Delta_{\delta}(U,U') = -\int d[\phi] d[\Pi] d[\Pi'] \min(e^{-E([\Pi,\Phi,U])},e^{-E([\Pi',\Phi,U'])}) \\ &\int d[U_{C}^{1}] \delta([\Pi,\Phi,U] - T_{MD}^{0}([\Pi_{1}^{-},\Phi,U_{C}^{1}])) \\ &\delta([\Pi_{1}^{+},\Phi,U_{C}^{1}] - T_{MD}^{1}([\Pi',\Phi,U'])) \delta(|(\eta,\Pi^{-})| - \sqrt{|4d|})(\eta,\Pi^{-}) \\ &\Delta_{\delta}(U',U) = -\int d[\phi] d[\Pi] d[\Pi'] \min\left(e^{-E([\Pi,\Phi,U])},e^{-E([\Pi',\Phi,U'])}\right) \\ &\int d[U_{C}^{1}] \delta([-\Pi',\Phi,U'] - \left(T_{MD}^{1}\right)^{-1}([-\Pi_{1}^{-},\Phi,U_{C}^{1}])) \\ &\delta([-\Pi_{1}^{+},\Phi,U_{C}^{1}] - \left(T_{MD}^{0}\right)^{-1}([-\Pi,\Phi,U])) \delta(|(\eta,\Pi^{-})| - \sqrt{|4d|})(\eta,-\Pi^{-}). \end{split} \tag{A.49}$$

Using the reversibility and area conservation of the molecular dynamics updates, it is clear that that  $\Delta_{\delta}(U,U')+\Delta_{\delta}(U',U)=0$ , and if we could guarantee that we only crossed once in the trajectory, the violation in detailed balance would be unimportant. However, when  $N_{\text{crossings}}>1$ , the terms which contain an even number of  $\delta(1+4d/(\eta,\Pi^-))$  functions will not cancel when we add  $\Delta_{\delta}(U,U')$  and  $\Delta_{\delta}(U',U)$ . If it is impossible that two of the  $\delta$ -functions can be satisfied simultaneously, this will not cause a problem, but given that the  $\delta$ -functions are only functions of one component of the momentum, it is not clear that this is the case.

We therefore feel that there is an argument that the Dirac  $\delta$  function in the Jacobian will cause a breakdown in the HMC, and a (currently) uncontrollable systematic error in any final results. However, this section should be seen as a work in progress, since we are not certain that this argument applies to

a numerical simulation. In a numerical simulation it is highly unlikely that we will ever hit the  $\delta$ -function. We also note that a non-zero Jacobian can be absorbed into the accept/reject step of the HMC [70], and that because the Jacobian (as we have written it) is not invertible there might be further difficulties. Until we have resolved this matter, we feel that it is best to use a (less efficient) update which does not have the  $\delta$ -function in the Jacobian.

Detailed balance will be satisfied either if the reflection condition x is a function of the gauge field at the crossing only, when the  $\delta$ -functions in  $\partial p/\partial \pi$  and  $\partial p/\partial r$  will exactly cancel when we calculate the Jacobian, or if there is no discontinuity between the transmission and reflection algorithms. The first of these possibilities does not guarantee that the square-root in the momentum update will be real; the second will either violate reversibility or energy conservation. In our algorithm, described in section 4, we combine these two possibilities in a way which ensures that energy conservation is only violated occasionally, that the square root is never imaginary, and that detailed balance is always satisfied.

By including the normal leapfrog algorithm as a third term in equation (A.39), it is easy to see that there is no problem with area conservation at the transition between the normal and corrected algorithms.

## A.3 The size of the correction step error

Suppose that there is a crossing between time  $\tau=0$  (where the gauge field, momentum, and fermionic force are  $U_0$ ,  $\Pi_0$  respectively), and time  $\tau=\Delta\tau$  (with gauge field  $U_1$ , momentum  $\Pi_1$ ). The gauge fields immediately before and after the eigenvalue crossing are  $U_d$  and  $U_u^8$ . If  $S(U)=E-\frac{1}{2}\Pi^2$  is the action, then the total force F' acting on the momentum is

$$f_i^{x\mu}(U) = \frac{\partial S(U)}{\partial r_i^{x\mu}} = -\frac{\partial \pi_i^{x\mu}}{\partial \tau}.$$
 (A.50)

In this section, we shall demonstrate that the energy difference,  $\Delta E$ , between time  $\tau = \Delta \tau$  and time  $\tau = 0$  is of order  $\Delta \tau^2$ . The energy change between time  $\Delta \tau$  and time 0 is

$$\Delta E = \frac{1}{2}(\Pi_1, \Pi_1) - \frac{1}{2}(\Pi_0, \Pi_0) + S(U_1) - S(U_0). \tag{A.51}$$

<sup>8</sup> Note that in practice  $U_u = U_d = U_c$  - there is no discontinuity in the gauge field at the crossing. The notation here is purely for clarification.

In this notation, our update for transmission (44, with  $s_1^2 = 1$ ), and neglecting terms of  $O(\Delta \tau^2)$  or higher is

$$\Pi^{-} = \Pi_{0} - \frac{\Delta \tau}{2} F_{0} 
\Pi^{+} = \Pi^{-} - \tau_{c} (1 - |\eta\rangle\langle\eta|) (F^{-} - F^{+}) + \tau_{c} \frac{1}{3} \text{Tr}(F^{-} - F^{+}) + 
\eta(\eta, \Pi^{-}) \sqrt{1 + \frac{4d}{(\eta, \Pi^{-})^{2}}} + 
\left(\eta_{1}^{2}(\eta_{1}^{2}, \Pi^{-} - \frac{\tau_{c}}{2}(F^{-} + F^{+})) + \eta_{2}^{2}(\eta_{2}^{2}, \Pi^{-} - \frac{\tau_{c}}{2}(F^{-} + F^{+}))\right) \times 
\left(\sqrt{1 - 2 \frac{\tau_{c}(F^{-}, \eta)(\Pi^{-}, \eta) - \tau_{c}(F^{+}, \eta)(\Pi^{+}, \eta)}{(\eta_{1}^{2}, \Pi^{-} - \frac{\tau_{c}}{2}(F^{-} + F^{+}))^{2}} - 1\right)} 
\Pi_{1} = \Pi^{+} - \frac{\Delta \tau}{2} F_{1} 
U^{-} = e^{i\frac{\Delta \tau}{2}\Pi^{-}} U_{0} 
U^{+} = e^{-i\tau_{c}\Pi^{+}} e^{+i\tau_{c}\Pi^{-}} U^{-} 
U_{1} = e^{i\frac{\Delta \tau}{2}\Pi^{+}} U^{+} 
U_{d} = e^{i(\frac{\Delta \tau}{2} + \tau_{c})\Pi^{-}} U_{0} 
U_{1} = e^{i(\frac{\Delta \tau}{2} - \tau_{c})\Pi^{+}} U_{u}.$$
(A.52)

There is a jump in the action S at the eigenvalue crossing,

$$S(U_u) - S(U_d) = -2d.$$
 (A.54)

Using  $(\Pi_+ - \Pi_-, F_+ - F_-) = O(\Delta \tau^2)$ , we can show that

$$(\Pi^{+}, \Pi^{+}) - (\Pi^{-}, \Pi^{-}) = 4d + 2\tau_{c}(\Pi^{-}, F^{+}) - 2\tau_{c}(\Pi^{-}, F^{-}) + \tau_{c}(\Pi_{+} - \Pi_{-}, F_{+} + F_{-}) + O(\Delta\tau^{2})$$
$$= 4d + 2\tau_{c}(\Pi^{-}, F^{+}) - 2\tau_{c}(\Pi^{-}, F^{-}) + O(\Delta\tau^{2}), \quad (A.55)$$

$$(\Pi_1, \Pi_1) - (\Pi_0, \Pi_0) = 4d - \Delta \tau ((\Pi_0, F_0) + (\Pi_1, F_1)) - 2\tau_c((F_0, \Pi^-) - (F_1, \Pi^+)) + O(\Delta \tau^2), \quad (A.56)$$

$$S(U_{1}) - S(U_{0}) = S\left(U\left(r_{ci}^{+} + \left(\frac{\Delta\tau}{2} - \tau_{c}\right)p_{i}\right)\right)$$

$$-S\left(U\left(r_{ci}^{-} + \left(\frac{\Delta\tau}{2} + \tau_{c}\right)\pi_{i}\right)\right) + O(\Delta\tau^{2})$$

$$= S(U_{u}) - S(U_{d}) + \left(\frac{\Delta\tau}{2} - \tau_{c}\right)\frac{\partial S}{\partial r_{i}}\Big|_{r_{c}^{+}}p_{i} + \left(\frac{\Delta\tau}{2} + \tau_{c}\right)\frac{\partial S}{\partial r_{i}}\Big|_{r_{c}^{-}}\pi_{i} + O(\Delta\tau^{2})$$

$$= -2d + \frac{\Delta\tau}{2}\left((\Pi^{+}, F_{1}) + (\Pi^{-}, F_{0})\right) + \tau_{c}((\Pi^{-}, F^{-}) - (\Pi^{+}, F^{+})) + O(\Delta\tau^{2}). \tag{A.57}$$

So,

$$\Delta E = O(\Delta \tau^2). \tag{A.58}$$

Therefore, our modified correction update for transmission conserves energy up to  $O(\Delta \tau^2)$ . Similarly, it can be shown that the energy violating reflection term is also  $O(\Delta \tau^2)$ . Without the additional  $\eta_4$ ,  $\eta_3$  correction, the energy violation would be

$$\frac{\tau_c}{2} \left( \left( F^- - F^+, \eta \right) (\Pi^- + \Pi^+, \eta) - \left( F^- + F^+, \eta \right) (\Pi^- - \Pi^+, \eta) \right) + O(\Delta \tau^2). \tag{A.59}$$

# B Two crossings in a molecular dynamics step

The case when two crossings occur in the same time step in opposite directions requires a little extra consideration. In sections 2.2 - 4, we assumed that the eigenvalues of the Dirac operator were not degenerate. If the eigenvalues are degenerate, then the eigenvectors can mix, and this process can affect the energy difference at the crossing if two eigenvalues should cross the zero axis at the same time (this occurred roughly once every 30 trajectories on our lowest mass  $4^4$  ensemble, and is less frequent on our higher mass ensembles, and more frequent on our  $8^4$  ensembles). Spotting when this has occurred on the computer is an additional problem, and we have not found an entirely robust method; currently we use equation (45) to estimate  $\tau_c$  for both the original and updated gauge fields, and therefore determine whether there have been any crossings in the time step.

We define  $|\psi_1^-\rangle$  and  $|\psi_2^-\rangle$  as the two "small" eigenvectors just before a crossing, and  $|\psi_1^+\rangle$  and  $|\psi_2^+\rangle$  as the eigenvectors just after the crossing.  $|\psi_1^+\rangle$  and  $|\psi_2^+\rangle$  will be linear combinations of  $|\psi_1^-\rangle$  and  $|\psi_2^-\rangle$ , and to preserve the orthonormality of the eigenvectors, the matrix mapping  $|\psi_1^-\rangle$  and  $|\psi_2^-\rangle$  to  $|\psi_1^+\rangle$ 

and  $|\psi_2^+\rangle$  must belong to U(2). Given that we are free to choose the phases of  $|\psi_1^+\rangle$  and  $|\psi_2^+\rangle$ , we are left with two parameters to describe the mapping. One possible representation is:

$$\begin{pmatrix} |\psi_1^+\rangle \\ |\psi_2^+\rangle \end{pmatrix} = \begin{pmatrix} \cos\theta & -\sin\theta e^{-i\phi} \\ \sin\theta e^{i\phi} & \cos\theta \end{pmatrix} \begin{pmatrix} |\psi_1^-\rangle \\ |\psi_2^-\rangle \end{pmatrix}. \tag{B.1}$$

We can now solve the eigenvalue equations

$$(Q - \delta Q)|\psi_1^-\rangle = \lambda_1^-|\psi_1^-\rangle$$

$$(Q - \delta Q)|\psi_2^-\rangle = \lambda_2^-|\psi_2^-\rangle$$

$$(Q + \delta Q)|\psi_1^+\rangle = \lambda_1^+|\psi_1^+\rangle$$

$$(Q + \delta Q)|\psi_2^+\rangle = \lambda_2^+|\psi_2^+\rangle. \tag{B.2}$$

We write

$$\langle \psi_i^- | \delta Q | \psi_j^- \rangle = \delta Q_{ij}.$$
 (B.3)

Then the solution to B.2 is

$$\lambda_{2}^{+} = \frac{1}{2} \left( 2\delta Q_{22} + 2\delta Q_{11} + \lambda_{2}^{-} + \lambda_{1}^{-} + \sqrt{\left( 2\delta Q_{22} - 2\delta Q_{11} + \lambda_{2}^{-} - \lambda_{1}^{-} \right)^{2} + 16\delta Q_{21}\delta Q_{12}} \right)$$

$$\lambda_{1}^{+} = \frac{1}{2} \left( 2\delta Q_{22} + 2\delta Q_{11} + \lambda_{2}^{-} + \lambda_{1}^{-} - \sqrt{\left( 2\delta Q_{22} - 2\delta Q_{11} + \lambda_{2}^{-} - \lambda_{1}^{-} \right)^{2} + 16\delta Q_{21}\delta Q_{12}} \right)$$

$$\tan^{2} \theta = \frac{\left( 2\delta Q_{11} - \lambda_{1}^{+} + \lambda_{1}^{-} \right)^{2}}{\delta Q_{12}\delta Q_{21}}$$

$$e^{2i\phi} = \frac{\delta Q_{12}}{\delta Q_{21}}.$$
(B.4)

Or, taking  $\delta Q \to 0$  and then  $\lambda \to 0$ ,

$$\tan^{2}\theta = \frac{\left(\dot{Q}_{22} - \dot{Q}_{11} - \operatorname{sign}(\dot{Q}_{22} - \dot{Q}_{11})\sqrt{(\dot{Q}_{22} - \dot{Q}_{11})^{2} + 4\dot{Q}_{12}\dot{Q}_{21}}\right)^{2}}{\dot{Q}_{12}\dot{Q}_{21}}$$

$$e^{2i\phi} = \frac{\dot{Q}_{12}}{\dot{Q}_{21}}.$$
(B.5)

The energy shift when these two eigenvalues cross can be calculated from

$$\frac{d}{d\tau} \Big[ |\psi_1\rangle \langle \psi_1| \operatorname{sign}(\lambda_1) + |\psi_2\rangle \langle \psi_2| \operatorname{sign}(\lambda_2) \Big].$$

Therefore, the energy shift is

$$\Delta E = -2d = (1 - \mu^2) \left( \langle X_1 | \gamma_5 S | X_2 \rangle + \langle X_1 | S \gamma_5 | X_2 \rangle \right)$$

$$S = \operatorname{sign}(\lambda_1^-) \left( |\psi_1^+\rangle \langle \psi_1^+| + |\psi_1^-\rangle \langle \psi_1^-| \right) + \operatorname{sign}(\lambda_2^-) \left( |\psi_2^+\rangle \langle \psi_2^+| + |\psi_2^-\rangle \langle \psi_2^-| \right)$$

$$= |\psi_1^-\rangle \langle \psi_1^-| \operatorname{sign}(\lambda_1^-) (1 + \cos 2\theta) + |\psi_2^-\rangle \langle \psi_2^-| \operatorname{sign}(\lambda_2^-) (1 + \cos 2\theta) - \operatorname{sin} 2\theta \left( |\psi_1^-\rangle \langle \psi_2^-| e^{-i\phi} + |\psi_2^-\rangle \langle \psi_1^-| e^{i\phi} \right). \tag{B.6}$$

Once d has been calculated, it can be inserted into the formulae in section 4, except that  $\tau_c$  should be the time at which the two smallest eigenvalues cross (to ensure that we maintain reversibility), and  $\eta$  therefore should be normal to the surface where the two eigenvalues are equal.

#### References

- [1] A. Frommer, Th. Lippert, B. Medeke, and K. Schilling (Eds.), Numerical Challenges in Lattice Quantum Chromodynamics, Lecture Notes in Computational Science and Engineering, Springer Verlag, Heidelberg, 2000, proceedings of the International Workshop, University of Wuppertal, August 22-24, 1999.
- [2] D. B. Kaplan, A Method for simulating chiral fermions on the lattice, Phys. Lett. B288 (1992) 342–347, hep-lat/9206013.
- [3] H. B. Nielson and B. Ninomiya, Nucl. Phys B185 (1981) 20.
- [4] R. Narayanan and H. Neuberger, Chiral fermions on the lattice, Phys. Rev. Lett. 71 (1993) 3251–3254, hep-lat/9308011.
- [5] H. Neuberger, Exactly massless quarks on the lattice, Phys. Lett. B417 (1998) 141–144, hep-lat/9707022.
- [6] P. Hasenfratz, Prospects for perfect actions., Nucl. Phys. Proc. Suppl. 63 (1998) 53–58, hep-lat/9709110.
- [7] P. H. Ginsparg and K. G. Wilson, A remnant of chiral symetry on the lattice, Phys. Rev. D25 (1982) 2649.
- [8] M. Lüscher, Abelian chiral gauge theories on the lattice with exact gauge invariance, Nucl. Phys. B549 (1999) 295–334, hep-lat/9811032.
- [9] P. Hernández, K. Jansen, and L. Lellouch, Finite-size scaling of the quark condensate in quenched lattice QCD, Phys. Lett. B469 (1999) 198–204, heplat/9907022.
- [10] P. Hernández, K. Jansen, and L. Lellouch, Chiral symmetry breaking from Ginsparg-Wilson fermions, Nucl. Phys. Proc. Suppl. 83 (2000) 633–635, heplat/9909026.

- [11] P. Hernández, K. Jansen, and L. Lellouch, A Numerical treatment of Neuberger's Lattice Dirac Operator, in: Frommer et al. [1], pp. 29–39, proceedings of the International Workshop, University of Wuppertal, August 22-24, 1999.
- [12] B. Bunk, hep-lat/9805030 (1998).
- [13] P. Hernández, K. Jansen, and M. Lüscher, A note on the practical feasibility of domain-wall fermions, hep-lat/0007015 (2000).
- [14] A. Boriçi, Fast methods for computing the Neuberger operator, in: Frommer et al. [1], pp. 40–47, proceedings of the International Workshop, University of Wuppertal, August 22-24, 1999.
- [15] A. Boriçi, A Lanczos approach to the inverse square root of a large and sparse matrix, J. Comput. Phys. 162 (2000) 123, hep-lat/9910045.
- [16] A. Boriçi, On the Neuberger overlap operator, Phys. Lett. B453 (1999) 46–53, hep-lat/9810064.
- [17] H. A. van der Vorst, Solution of f(A)x = b with Projection Methods, in: Frommer et al. [1], pp. 18–28, proceedings of the International Workshop, University of Wuppertal, August 22-24, 1999.
- [18] H. Neuberger, A practical implementation of the overlap-Dirac operator, Phys. Rev. Lett. 81 (1998) 4060–4062, hep-lat/9806025.
- [19] H. Neuberger, Overlap Dirac Operator, in: Frommer et al. [1], proceedings of the International Workshop, University of Wuppertal, August 22-24, 1999.
- [20] R. G. Edwards, U. M. Heller, J. Kiskis, and R. Narayanan, Chiral condensate in the deconfined phase of quenched gauge theories, Phys. Rev. D61 (2000) 074504, hep-lat/9910041.
- [21] R. G. Edwards, U. M. Heller, and R. Narayanan, A study of practical implementations of the overlap-Dirac operator in four dimensions, Nucl. Phys. B540 (1999) 457–471, hep-lat/9807017.
- [22] J. van den Eshof, A. Frommer, Th. Lippert, K. Schilling, and H.A. van de Vorst, Numerical Methods for the QCD overlap Operator: I. Sign-Function and Error Bounds, Comput. Phys. Comm. 146 (2002) 203–224.
- [23] R. V. Gavai, S. Gupta, and R. Lacaze, Speed and adaptability of overlap fermion algorithms, Comput. Phys. Commun. 154 (2003) 143–158, hep-lat/0207005.
- [24] S. J. Dong et al., Chiral logs in quenched QCD, hep-lat/0304005.
- [25] T. Chiu, T. Hsieh, C. Huang, and T. Huang, A note on the Zolotarev optimal rational approximation for the overlap Dirac operator, phys. Rev. D66 (2002) 114502, hep-lat/0206007.
- [26] Z. Fodor, S. D. Katz, and K. K. Szabo, Dynamical overlap fermions, results with hybrid Monte-Carlo algorithm, JHEP 08 (2004) 003, hep-lat/0311010.

- [27] T. Chiu, Optimal domain-wall fermions, Phys. Rev. Lett. 90 (2003) 071601, hep-lat/0209153.
- [28] T. Chiu, Locality of optimal lattice domain-wall fermions, Phys. Lett. B552 (2003) 97–100, hep-lat/0211032.
- [29] T. Chiu, Optimal lattice domain-wall fermions with finite N(s), hep-lat/0304002 (2003).
- [30] A. Borici, A. D. Kennedy, B. J. Pendleton, and U. Wenger, The overlap operator as a continued fraction, Nucl. Phys. Proc. Suppl. 106 (2002) 757–759, heplat/0110070.
- [31] H. Neuberger, The overlap lattice Dirac operator and dynamical fermions, Phys. Rev. D60 (1999) 065006, hep-lat/9901003.
- [32] U. Wenger, The overlap Dirac operator as a continued fraction. Hep-lat/0403003.
- [33] C. Liu, Hybrid Monte Carlo algorithm for lattice QCD with two flavors of dynamical Ginsparg-Wilson quarks, Nucl. Phys. B554 (1999) 313–322, heplat/9811008.
- [34] P. Hernández, K. Jansen, and L. Lellouch, A numerical treatment of Neuberger's lattice Dirac operator, in: A. Frommer (Ed.), Wuppertal 1999, Numerical challenges in lattice quantum chromodynamics, 2000, pp. 29–39, hep-lat/0001008.
- [35] K. Jansen, Overlap and domain wall fermions: What is the price of chirality?, Nucl. Phys. Proc. Suppl. 106 (2002) 191–192, hep-lat/0111062.
- [36] L. Giusti, C. Hoelbling, and C. Rebbi, Light quark masses with overlap fermions in quenched QCD, Phys. Rev. D64 (2001) 114508, hep-lat/0108007.
- [37] L. Giusti, C. Hoelbling, M. Lüscher, and H. Wittig, Numerical techniques for lattice QCD in the epsilon- regime, Comput. Phys. Commun. 153 (2003) 31–51, hep-lat/0212012.
- [38] S. Duane, A. Kennedy, B. Pendelton, and D. Roweth, Phys. Lett. B195 (1987) 216.
- [39] S. Dürr, Ch. Hoelbling, and U. Wenger, A comparative study of overlap and staggered fermions in QCD Hep-lat/0409108.
- [40] S. Dürr and Ch. Hoelbling, Staggered versus overlap fermions: A study in the Schwinger model with N(f)=0.1,2, Phys. Rev. D69 (2004) 034503, hep-lat/0311002.
- [41] L. Giusti, Ch. Hoelbling, and C. Rebbi, Schwinger model with the overlap-Dirac operator: Exact results versus a physics motivated approximation, Phys. Rev. D64 (2001) 054501, hep-lat/0101015.

- [42] A. Bode, U. M. Heller, R. G. Edwards, and R. Narayanan, First experiences with HMC for dynamical overlap fermions, in: Dubna 1999, Lattice fermions and structure of the vacuum, 1999, pp. 65–68, hep-lat/9912043.
- [43] S. Dürr and C. Hoelbling, Scaling tests with dynamical overlap and rooted staggered fermions Hep-lat/0411022.
- [44] Z. Fodor, S. D. Katz, and K. K. Szabo, Dynamical overlap fermions, results with HMC algorithm, Nucl. Phys. Proc. supp. 140C, hep-lat/0409070.
- [45] T. DeGrand and S. Schaefer, Physics issues in simulations with dynamical overlap fermions Hep-lat/0412005.
- [46] P. Hernandez, K. Jansen, and M. Lüscher, Locality properties of Neuberger's lattice Dirac operator, Nucl. Phys. B552 (1999) 363–378, hep-lat/9808010.
- [47] G. Arnold, N. Cundy, J. van den Eshof, A. Frommer, S. Krieg, Th. Lippert, and K. Schäfer, Numerical methods for the QCD overlap operator. II: Optimal Krylov subspace methods To appear in the proceedings of the Third International Workshop on Numerical Analysis and Lattice QCD, hep-lat/0311025.
- [48] N. Cundy, J. van den Eshof, A. Frommer, S. Krieg, Th. Lippert, and K. Schäfer, Numerical methods for the QCD overlap operator. III: Nested iterations., Comp. Phys. Comm. 165 (2005) 841, hep-lat/0405003.
- [49] S. Krieg et al., Improving inversions of the overlap operator, Nucl. Phys. Proc. supp. 140C, hep-lat/0409030.
- [50] N. Cundy, S. Krieg, A. Frommer, Th. Lippert, and K. Schilling, Dynamical overlap simulations using HMC, Nucl. Phys. Proc. supp. 140C (2005) 841, heplat/0409029.
- [51] S. Gottlieb, W. Liu, D. Tossaint, R. L. Renken, and R. L. Sugar, Hybrid-molecular-dynamics algorithms for the numerical simulation of quantum chromodynamics, Phys. Rev. D35 (1987) 2531.
- [52] D. Ingerman, V. Druskin, and L. Knizerhman, Comm. Pure Appl. Math. 53 (2000) 1039.
- [53] P. P. Petrushev and V. A. Popov, Rational approximation of real functions, Cambridge University Press, 1987.
- [54] R. P. Brent, Algorithms for minimization without Derivitives, Englewood Cliffs, NJ, 1973.
- [55] W. Press, S. Teukolsky, W. Vetterling, and B. Flannery, Numerical Recipies in Fortran, 2nd Ed., Cambridge University Press, 1992.
- [56] H. Neff, Efficient computation of low-lying eigenmodes of non-Hermitian Wilson-Dirac type matrices, Nucl. Phys. Proc. Suppl. 106 (2002) 1055–1057, hep-lat/0110076.

- [57] http://www.caam.rice.edu/software/ARPACK/.
- [58] T. Kalkreuter and H. Simma, An Accelerated conjugate gradient algorithm to compute low lying eigenvalues: A Study for the Dirac operator in SU(2) lattice QCD, Comput. Phys. Commun. 93 (1996) 33–47, hep-lat/9507023.
- [59] N. Garron, L. Giusti, Ch. Hoelbling, L. Lellouch, and C. Rebbi, B(K) from quenched QCD with exact chiral symmetry, Phys. Rev. Lett. 92 (2004) 042001, hep-ph/0306295.
- [60] R. G. Edwards, U. M. Heller, and R. Narayanan, The overlap-Dirac operator: Topology and chiral symmetry breaking, Chin. J. Phys. 38 (2000) 594–604, hep-lat/0001013.
- [61] R. G. Edwards, U. M. Heller, and R. Narayanan, A study of practical implementations of the overlap-Dirac operator in four dimensions, Nucl. Phys. B540 (1999) 457–471, hep-lat/9807017.
- [62] Z. Fodor, personal Communication.
- [63] R. J. Crewther, Phys.Lett. B70 (1977) 349.
- [64] P. Di Vecchia and G. Veneziano, Nucl Phys B171 (1980) 253.
- [65] H. Leutwyler and A. Smilga, Phys. Rev. D45 (1992) 5607.
- [66] C. Bernard et al., Topological susceptibility with the improved Asqtad action, Phys. Rev. D68 (2003) 114501, hep-lat/0308019.
- [67] G. S. Bali et al., Quark mass effects on the topological susceptibility in QCD, Phys. Rev. D64 (2001) 054502, hep-lat/0102002.
- [68] S. Dürr, Topological susceptibility in full QCD: Lattice results versus the prediction from the QCD partition function with granularity, Nucl. Phys. B611 (2001) 281–310, hep-lat/0103011.
- [69] I. Montvay and G Münster, Quantum Fields on a Lattice, 1994.
- [70] A. Borici, private communication.